

Spectroscopy with trapped francium: advances and perspectives for weak interaction studies

E Gomez¹, L A Orozco² and G D Sprouse¹

¹ Department of Physics and Astronomy, State University of New York at Stony Brook, Stony Brook, NY 11794-3800, USA

² Department of Physics, University of Maryland, College Park, MD 20742-4111, USA

E-mail: lorozco@umd.edu

Received 10 August 2005, in final form 3 October 2005

Published 7 November 2005

Online at stacks.iop.org/RoPP/69/79

Abstract

Francium is a candidate for atomic parity non-conservation (PNC) experiments. Its simple atomic structure has been the subject of extensive experimental research facilitated by the ability to trap and cool significant numbers of atoms. The studies include the location of energy levels, their hyperfine splittings and their lifetime. All of these levels are close to the ground state. The results show a remarkable agreement with calculated *ab initio* properties to a degree that is comparable with other stable alkali atoms. The quantitative understanding of francium has made possible the exploration of avenues for a PNC measurement in the optical and the microwave regimes. These precision experiments have the potential to enhance our understanding of the weak coupling constants between electrons and nucleons, as well as between nucleons.

Contents

	Page
1. Introduction	81
2. Francium production and trapping	82
2.1. Francium production	82
2.1.1. Decay techniques	82
2.1.2. Accelerator sources	82
2.2. The francium trap	86
2.2.1. Cell coatings	86
2.2.2. The Stony Brook first trap	86
2.2.3. The Boulder trap	88
2.2.4. The Legnaro trap	88
2.2.5. The Stony Brook second trap	89
2.3. Trapping efficiency for radioactive atoms	91
3. Spectroscopy of Fr	91
3.1. Experiments	92
3.1.1. Energy levels	92
3.1.2. ^{221}Fr 7p levels	95
3.1.3. Hyperfine anomaly	96
3.1.4. Lifetime measurements	97
3.2. Atomic structure of francium	104
4. Parity non-conservation	106
4.1. Atomic PNC theoretical background	107
4.2. The anapole moment	108
4.3. Status of PNC measurements	109
5. Considerations for a PNC experiment in francium	110
5.1. The optical experiment	110
5.2. The anapole moment measurement	112
5.3. Other optical atomic PNC proposals	113
6. Perspectives and conclusions	113
Acknowledgments	113
Appendix. Tables of Fr parameters	113
References	115

1. Introduction

Francium is the heaviest of the alkali atoms, so it has both a simple electronic structure and a large nucleus. All its isotopes are radioactive and the longest lived isotope has a half-life of 21.8 min. The advent of laser trapping and cooling [1] opened the possibility to study its properties in a controlled environment. Trapping of radioactive atoms has become a field in itself [2]. It is closely related to weak interaction studies; in particular, precision measurements based on beta-decay of samples of atoms [3–5].

The long-term goal of the measurements in francium reviewed here is to reach a quantitative understanding that will permit the study of the weak interaction through a parity non-conservation (PNC) measurement. Although no experiment has been completed to date, various groups are preparing to undertake the study of PNC in francium. This review focuses on the measurements of the atomic structure of Fr and some of the existing experimental proposals for atomic PNC studies in Fr. There are extensive reviews on the theoretical methods associated with atomic PNC by the two leading theoretical groups in the field [6, 7] with details on the current state of the calculations. The review by Bouchiat and Bouchiat [8] presents the state of atomic PNC experiments in 1997.

The pioneering work of Bouchiat and Bouchiat [9] recognized that the size of the effect of PNC in atoms scales faster than Z^3 , with Z the atomic number, launching a series of experiments to look for effects of the weak interaction in heavy atoms. This strong scaling has made it possible not only to observe PNC effects in atoms but also to measure weak interaction coupling constants.

Atomic PNC work has been centred around heavy atoms with atomic number greater than 50 [10–14]. Recent measurements in Cs [10] have reached sensitivity to the nuclear spin dependent part of the interaction (primarily due to the nuclear anapole moment), opening a new avenue for studies of the weak interaction within the nucleus [15, 16], an area very difficult to probe otherwise.

On the other hand, the spin independent measurements, helped by the *ab initio* atomic physics calculations [17, 18], have been used to put constraints on physics beyond the Standard Model [19]. Recent analysis of the results [20–22] show that an atomic PNC measurement can place limits in the masses of extra neutral gauge bosons. However, the atomic and nuclear theory calculations are sufficiently complicated that high order corrections previously neglected [23] can modify the high energy limits obtained from the atomic PNC results.

The road to a PNC measurement in francium is long and several intermediate steps have to be completed before getting there. The first step was achieved by the group of Liberman [24] when they managed to locate the $7S_{1/2} \rightarrow 7P_{3/2}$ transition, the so called D_2 line of francium at CERN. The steady progress in the electronic and nuclear properties of francium was fundamental for the 1995 magneto-optical trapping on line with the superconducting linear accelerator at Stony Brook [25]. The new ability to make and contain francium provided a sample of about 10^3 cold atoms confined to a interaction free region, ready to be studied. The Stony Brook group has devoted several years to the understanding of the electronic structure through spectroscopy. The study included the identification of energy levels and hyperfine splitting measurements [26–29] and the measurement of electronic level lifetimes [30–34]. The measurements provide complementary information on the electronic structure near the nucleus and far away from it. The Wieman group at Boulder succeeded in trapping francium that came as a daughter in the radioactive decay of ^{229}Th and studied the electronic structure and hyperfine splittings of ^{221}Fr [35]. Recent advances at the accelerator in Legnaro, Italy led by Moi have opened a new source for the continuation of research with francium [36].

2. Francium production and trapping

Perey [37], of the Curie Institute in Paris, reported in 1939 the discovery of a new radioactive element. While doing chemical analysis of the decay products of actinium, she found an element that behaved as an alkali. She named the new element francium after her country.

Francium is the heaviest of the alkali elements, with 87 electrons. It is the most unstable of the first 103 elements, with isotopes containing between 201 and 230 nucleons. In the last three decades, states with energies accessible by laser excitation were measured in pioneering work at ISOLDE in CERN [38]. Their measurements of hyperfine splittings revealed information about the nuclear structure of the francium isotopes 207–213 and 220–228 [39]. Andreev *et al* [40] studied the structure of two Rydberg series including the ionization potential using ^{221}Fr , a daughter product of the decay of ^{229}Th , by laser-resonance ionization.

It is now possible to perform precise measurements of the atomic properties of francium as a result of two different developments. First new targets are available for its production with more selective nuclear fusion reactions and second the advent of laser trapping and cooling techniques for on-line capture of the produced radioactive isotopes [2].

2.1. Francium production

The simplest way to obtain francium is from a natural source. The short lifetime of francium makes it hard to find it naturally in large amounts. The other approach is to produce the radioactive element in an accelerator. This implies the selection of a fusion or spallation reaction, the preparation of an appropriate beam and target as well as a means of extracting and directing the francium to a different area for the spectroscopic measurements.

2.1.1. Decay techniques. The most common method used to obtain a sample of ^{221}Fr starts with a radioactive source of ^{229}Th ($\tau_{1/2} = 7340$ yr), which alpha decays into ^{225}Ra ($\tau_{1/2} = 14.9$ d). The Ra then beta decays into ^{225}Ac ($\tau_{1/2} = 10$ d) which alpha decays to produce the ^{221}Fr ($\tau_{1/2} = 4.9$ min). The group of Lethokhov produced a foil containing ^{221}Fr by starting with a thin layer of ^{229}Th . They placed a thin Ta foil directly on top of the Th activity, so that the recoil momentum of the first alpha decay would propel some of the ^{225}Ra into the Ta foil. After several weeks of close contact with the Th activity, the Ta foil was placed in the experiment and heated to release the ^{221}Fr activity that accumulates from the subsequent decays [40]. The Wieman group deposited actinium in a platinum ribbon either electroplating it from a thorium solution or via electrostatic collection of radium in a helium atmosphere [35]. They placed the platinum inside an orthotropic oven to produce a highly collimated beam of about 10^4 ^{221}Fr atoms/s [41]. The advantage of the decay method is that it does not require an accelerator to produce francium. The disadvantage is the limited number of atoms and isotopes produced this way.

2.1.2. Accelerator sources. The pioneering work of Liberman *et al* [24] relied on an accelerator source at CERN to produce francium in spallation reactions. At Stony Brook and Legnaro, heavy ion fusion reactions produce the light francium isotopes.

Spallation sources. Copious amounts of francium have been produced at the ISOLDE experiment at CERN [42]. High energy protons (originally 0.6 GeV and now 1.4 GeV) impinge on 50–100 g cm^{-2} ThC and UC targets to produce $>10^9$ atoms/ μC for $^{208-212, 220-226}\text{Fr}$ and lesser amounts of other isotopes. Spallation reactions produce these francium isotopes, but

fission reactions make a tremendous amount of other activity. The target is heated to have quick diffusion and rapid release of the volatile elements such as francium. Target materials must withstand the large beam power, but yet allow a short diffusion path for the activity to reach the surface of the target material, and then quickly diffuse to the ionization region. After ionization and acceleration to 60 keV, the different isotopes of Fr are magnetically separated from all other activities and sent to the experiment. Typical proton beam intensities at ISOLDE have been 1–10 μA limited mainly by radiation safety concerns. The ISAC facility at TRIUMF in Vancouver, B.C. Canada is currently developing targets for 100 μA of 500 MeV protons. ISAC and other proposed facilities such as the Rare Isotope Accelerator hope to have even more intense sources of Fr and other elements.

Fusion sources. Another alternative to produce unstable nuclei is with heavy-ion fusion reactions. A beam projectile with enough energy can overcome the Coulomb repulsion of the two nuclei and fuse them to form a compound nucleus. The new nucleus cools down by boiling off neutrons, creating a different isotope. The fusion reaction is more selective than the spallation reactions, and projectile–target–energy combinations can be chosen so that more than half of the reaction cross section forms a particular isotope, eliminating the need for magnetic separation of reaction products. Different combinations of target and projectile can make the same isotope, e.g. ^{12}C on ^{203}Tl or ^{18}O on ^{197}Au both make the same compound nucleus, ^{215}Fr , but the Au target is much to be preferred because of its chemical properties of noble metal and its low vapour pressure near the melting point. This latter reaction has been used at Stony Brook and Legnaro to produce ^{210}Fr . The products come to a stop in the target. As the target is heated, the reaction products, diffuse to the surface, are surface-ionized and are transported as ions to a region where after neutralization they are trapped in a magneto optical trap (MOT) for further measurements.

The apparatus used to trap francium at Stony Brook is based on the same principles as the one they used to trap radioactive ^{79}Rb [43]. Beams of ^{18}O from the Stony Brook superconducting LINAC are incident on a Au target mounted on a W rod. The $^{197}\text{Au}(^{18}\text{O},xn)$ reaction at 100 MeV produces predominantly ^{210}Fr , which has a 3.2 min half-life. ^{210}Fr has an estimated α decay branching of $60 \pm 30\%$ with the remaining decays by β^+ or electron capture. The target is heated to $\approx 1200\text{ K}$ by the beam power and by an auxiliary resistance heater as seen in figure 1. The francium is surface ionized as it escapes from the gold because the work function of gold (4.8–5.1 eV) is larger than the ionization potential of francium (4.07 eV).

A beam energy of 100 MeV is optimal for production of ^{210}Fr since this isotope is created very close to the surface facilitating its escape from the target. Changing the beam energy modifies the production rate of the francium isotopes. Increasing the beam energy allows the francium nucleus to expel more neutrons during the cooling process following nuclear fusion. This produces francium isotopes with fewer neutrons. Combinations of projectile energy and targets have allowed the production and trapping of $^{208-212}\text{Fr}$ at Stony Brook [28]. To produce and trap ^{212}Fr , they used an isotopically enriched Pt target with a beam of ^{19}F [44]. Its 19.6 min half-life makes it nearly the longest lived francium isotope.

Close to the melting point of gold (1336 K) the Fr diffuses the most rapidly but the structural properties of the Au may become unstable. The coil around the W rod and the beam current heated the target, and there was a sensitive dependence of the number of francium ions on the target temperature. The elevated temperature is necessary for the alkali elements to rapidly diffuse to the surface and be surface ionized [45]. There was a sharp increase in the number of francium ions that escaped from a new gold target when it heated. Figure 2 plots the alpha decay rate of francium ions at the silicon detector as a function of time while the beam is on the target. Increasing the ^{18}O beam current prior to the sharp transition had little effect on

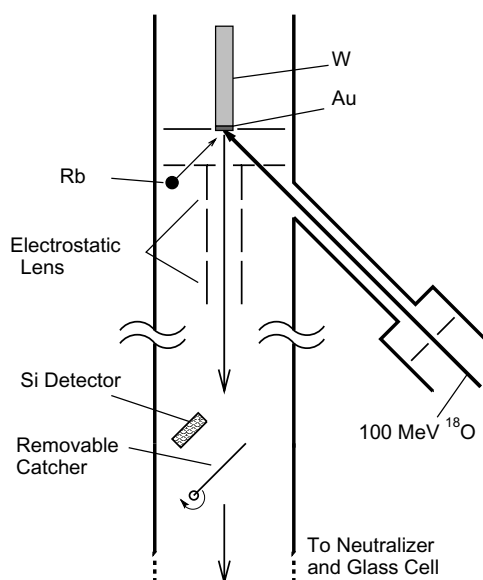


Figure 1. Schematic view of target and ion transport system from the first Stony Brook apparatus (figure taken from [25]).

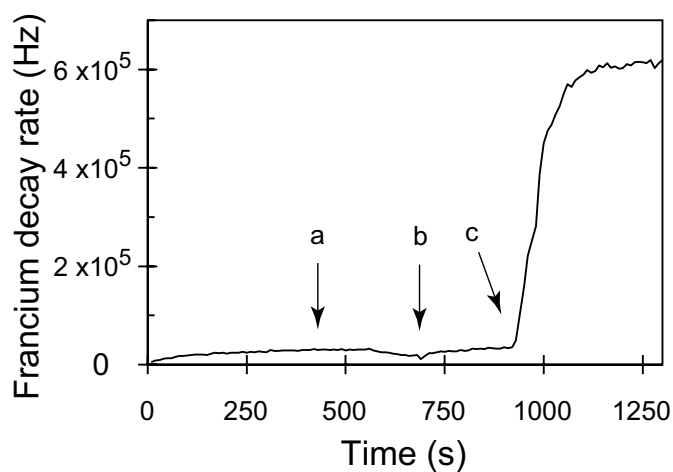


Figure 2. Francium alpha-particle decay rate at the catcher in the ion transport system versus time at Stony Brook. The decay rate reaches an equilibrium at point (a). Increasing the beam current has little effect on the production rate at point (b). At point (c), the target heating is increased and the transition occurs.

the francium escape rate (see figure 2(b)). Once the transition was reached, a large increase in the francium escape rate occurred (see figure 2(c)). While the behaviour is not completely understood, it seems that the target may be locally melting at the point where the beam hits the gold. The transition can be repeated with a single target although the increase is less dramatic after several cycles. The behaviour may be caused by the removal of impurities from the gold surface that prevent surface ionization of the francium. Images taken of a new target show the

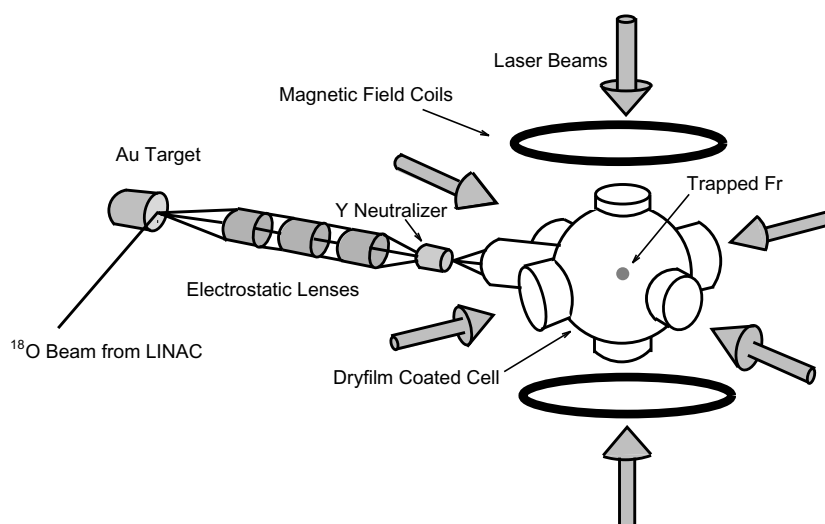


Figure 3. Schematic view of target, ion transport system and MOT for the first generation Stony Brook apparatus (figure taken from [31]).

region of melting because the emissivity of the liquid is about 5% larger than that of the solid. Such changes always coincide with the increase in alpha production.

Francium ion transport and neutralization. The francium ions entered the ion transport system shown in figure 1. The cylindrically symmetric target and electrodes reduced aberrations. The ions were extracted at 135° from the ^{18}O beam direction. A retractable plate (catcher) facing a silicon surface-barrier detector stops the Fr beam and measures the number of Fr decays to obtain the flux. The alpha-particle activity and the known solid angle of the detector determine the number of francium atoms in the beam. The different alpha energies and lifetimes allow isotope identification. A beam from the Stony Brook Superconducting LINAC of 6×10^{11} ^{18}O ions/s on the Au produced $\approx 1 \times 10^6$ ^{210}Fr ions/s at the catcher.

The apparatus shown in figure 3 separated the production and the trapping regions. This was critical to operate the trap in an ultra-high vacuum environment. Extracted at around 800 V, the francium ions travelled through three sets of electrostatic lenses that focused the ions and three sets of electrostatic plates steered them. The ion transport system was all electrostatic to be mass independent. This permitted fine tuning of the system with a stable Rb beam generated by the dispenser next to the target shown in figure 1. The similarity of the ionization potential and neutralization properties of Rb and Fr made the choice of Rb ideal for further studies of the apparatus including the laser trap downstream. After about 1 m, the ions passed through a differential-pumping aperture to the region of ultra-high vacuum. The ions were deposited on the inner surface of a cylinder coated with yttrium and heated to 970 K (melting point of Y = 1752 K). The low work function of Y (3.1 eV) results in the release of neutral Fr atoms from the Y surface that form an atomic beam directed towards the vapour cell MOT.

The neutralizer must be made of a material with a work function smaller than the ionization potential of francium (4.07 eV). Yttrium, zirconium and thoriated tungsten are among the materials with such a characteristic. The release time of francium in the neutralizer must be fast and with low outgassing to decrease any damage to the vacuum or the dry film coating. For a recent study of different materials as neutralizers see [46].

2.2. The francium trap

The vapour cell MOT developed by the group of Wieman [47] for stable alkali has many properties that makes it a great choice for trapping francium. The trap does not require any deceleration of the atoms before they enter the glass cell, such as that provided by a Zeeman decelerator for radioactive sodium [48]. The atoms collide with the walls and re-thermalize. The atoms in the slow end of the Maxwell–Boltzmann velocity distribution have low enough kinetic energy to be trapped. Fast atoms can still be trapped on a second or subsequent pass after re-thermalization with the cell walls. The trap requires special attention to the glass utilized for the vapour cell, as it is necessary to ensure that the atom does not stay on the wall, but is desorbed after a short time.

2.2.1. Cell coatings. On bare silica, pyrex or metal surfaces, alkalis stick with a probability close to one. This is due to two effects: chemisorption where the alkali atom undergoes a chemical reaction on the wall and is permanently removed from the vapour and physisorption where the atom is trapped in a potential well on the surface for an average time $\bar{\tau}_s$ and returns afterwards into the vapour. This results in a reduced vapour pressure inside the bulb.

Once a monolayer of alkali atoms has formed on the walls, the vapour pressure rises to its usual value. This does not pose a particular problem with stable isotopes, since a monolayer is easily applied. With production rates of radioactive alkalis of less than 10^{10} s^{-1} it is impossible to form such a monolayer ($\approx 10^{16}$ atoms on 100 cm^2 surface). A solution has been to find a surface coating which reduces chemisorption and physisorption. Such coatings have been investigated for use in hydrogen masers, Cs/Rb frequency standards and polarized targets [49, 50].

Possible coatings are hydrocarbon surfaces, such as dry film (silanes), polyethylene and paraffin. When properly applied, these chemicals form methyl groups on the host surface in such a way that the hydrogen atoms shield the incoming alkali atom from getting close and reacting with C, Si or O atoms deeper in the surface.

These coatings display low adsorption energies and reaction rates. The results vary from group to group and are sometimes contradictory. This might be caused by the extreme sensitivity of the coatings to cleaning procedures and different container geometries. Since a MOT requires a significantly better vacuum than some of the other applications of coatings such as masers and polarized targets, one has to pay special attention to the outgassing. Opacity and chemical reaction rates must be minimized too. The Stony Brook group used dry film for their first trap, using the procedure of Swenson and Anderson based on SC-77 [51]. It could be baked to at least 275°C . Reference [52] has a detailed study of different coatings done by the Boulder group. The Legnaro group has used a thin film of polydimethylsiloxane (PDMS) which serves two purposes: it prevents the atoms from sticking to the walls and enables desorption of the atoms with weak illumination. Using light-induced atomic desorption they have observed loading rates of $2 \times 10^8 \text{ s}^{-1}$ in a rubidium trap [53].

2.2.2. The Stony Brook first trap. Francium atoms left the yttrium neutralizer in a beam and entered the vapour cell shown in figure 3. The francium trap consisted of a 10 cm diameter Pyrex bulb with six 5 cm diameter windows and two viewing windows 3 cm in diameter. The MOT was formed by six intersecting laser beams each with $1/e^2$ (power) diameter of 4 cm and typical intensity of 7.8 mW cm^{-2} and a magnetic field gradient of $5.5 \times 10^{-2} \text{ T m}^{-1}$.

The atomic energy levels of the ^{210}Fr atom relevant for trapping are shown in figure 4. A laser excited the cycling transition $7S_{1/2}, F = 13/2 \rightarrow 7P_{3/2}, F = 15/2$ at 718 nm. The ^{210}Fr ground-state hyperfine splitting of 46.8 GHz requires an extra laser for repumping the

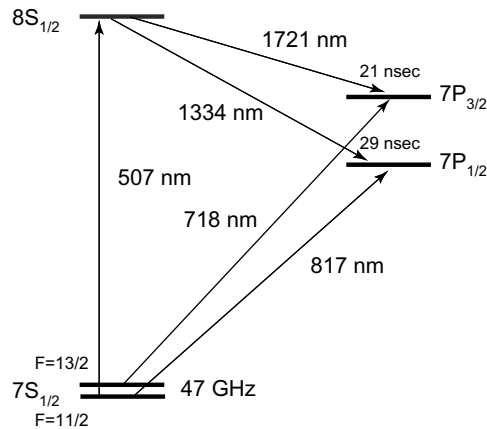


Figure 4. Relevant energy levels for trapping of francium and the forbidden electric dipole ($E1$) transition between $7s$ and $8s$ that can be used in a PNC measurement.

atoms that fall into the $F = 11/2$ ground state. Another laser tuned to the appropriate transition either to the $7P_{3/2}$ (718 nm) or $7P_{1/2}$ (817 nm) level can repump the atoms.

Absolute frequency references are necessary for the trapping lasers because there are no stable isotopes of Fr to use for this purpose. The atlas of the I_2 spectrum [54] provided the laser frequency calibration for the initial trapping experiment [25]. Later coarse absolute frequency determination ($\pm 0.001 \text{ cm}^{-1}$) was provided by a commercial wavemeter, and a computer-controlled scanning Fabry–Perot cavity allowed long term stabilization of the frequencies of all the lasers involved in the trapping and probing of francium [55, 56]. The system works by maintaining the relative distance of the fringes produced by the lasers compared with the fringes from a frequency stabilized HeNe laser. The cavity system could lock and adjust the laser frequency with a resolution of about 1 MHz at Stony Brook for many hours.

The Stony Brook group used lock-in detection to reject laser light scattered from the cell while measuring the fluorescence from the captured atoms. They frequency modulated (FM) the trapping laser at 14.5 kHz and collected the light with an $f/2$ optical system into a photomultiplier tube (PMT).

Before trapping Fr, the trapping apparatuses at Stony Brook, Legnaro and Boulder were tested extensively using stable elements. At Stony Brook they injected rubidium into the cell from the dispenser next to the Au target (see figure 1). The trapped Rb was used to optimize the position of the photomultiplier that detects the trapped atoms. Then to trap francium the only change was in the laser frequencies without further adjustment of the trap or detection optics.

Figure 5 shows the fluorescence signal from the captured francium atoms in the first Stony Brook trap. Panel (a) is a plot of the fluorescence signal of the trapped atoms as the trapping laser scanned over a 60 MHz range at 0.5 MHz s^{-1} . The fluorescence signal was integrated with a 1 s time constant. The asymmetry of the signal reflects the fact that the trap only works for red detuning (cooling side of transition). Panel (b) shows the fluorescence from trapped atoms with a different, wider, scan of the laser. Panel (c) corresponds to the shifted absorption (by 3.1 GHz) of the line 381 [54] of I_2 . For the wide scan two rates were used: around the centre of the scan 1.0 MHz s^{-1} , with a faster one elsewhere.

The parameters for a francium trap are summarized in the appendix in table 5.

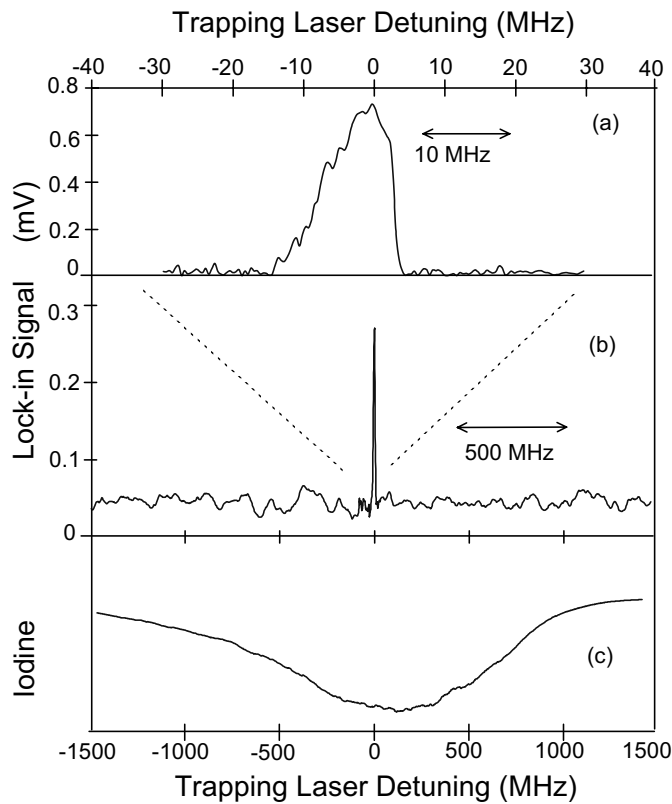


Figure 5. (a) Trap fluorescence versus frequency detuning (60 MHz scan), the centre corresponds to $13923.286 \pm 0.03 \text{ cm}^{-1}$. (b) Trap fluorescence versus frequency detuning (3.0 GHz scan). (c) I_2 absorption line (3.0 GHz scan) (figure adapted from [25]).

2.2.3. The Boulder trap. The Boulder group has followed the table top experimental approach. They used a decay source of ^{225}Ac implanted in a platinum ribbon. They installed the platinum inside an orthotropic oven to produce an atomic beam. The oven used a combination of a neutralizer and an ionizer to recycle the atoms except those already going in a highly collimated direction. They obtained about 10^4 ^{221}Fr atoms/s with a divergence smaller than 150 mrad [41].

The francium beam entered a quartz glass cube (4.4 cm inside dimension) through a 2 mm diameter hole in one of the corners (see figure 6). The cell walls had a dry film coating (SC-77) [52], and both the oven and cell were placed inside a vacuum chamber at 1.3×10^{-8} bar. Their detection system allowed them to resolve 15 trapped francium atoms ($1/\sqrt{s}$). They used 4 cm diameter, 18 mW cm^{-2} trap beams, 60 mW of repumper and a magnetic field gradient of $7.0 \times 10^{-2} \text{ T m}^{-1}$ to trap more than 900 francium atoms [35].

2.2.4. The Legnaro trap. The Istituto Nazionale di Fisica Nucleare, Legnaro laboratories, has set up a francium MOT [53, 57]. They produce francium in a nuclear reaction between an ^{18}O beam and a ^{197}Au target. An XTU-Tandem accelerator delivers the oxygen beam with an optimal energy of 104 MeV for ^{210}Fr production. They heat the gold target to 1300 K to help the francium diffuse out of the target. The target has a conical shape to minimize the ion beam

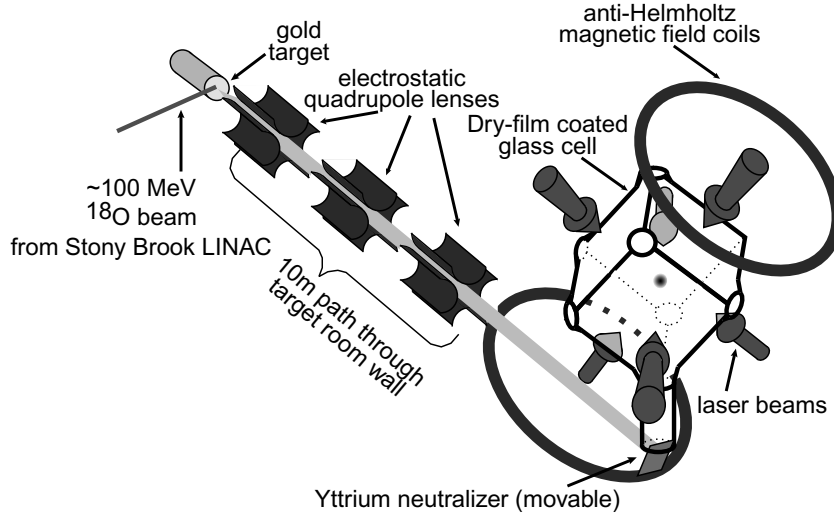


Figure 8. Second generation Stony Brook on-line apparatus for francium production and trapping. The drawing is not to scale (figure adapted from [58]).

The focus of the design was in three points: the optical trap, the neutralizer and the exit holes.

The optical trap efficiency depends on the capture velocity, which is the maximum velocity that an atom can have and still be trapped, and the trapping volume. The trapping volume should be as close to the total available volume as possible. To maximize the capture velocity it is necessary to increase the trap laser beams size, the detuning and the power. Since the power is fixed by the laser used, this also limits the optimum beam size and detuning. The cell consists of a cube (5 cm on the side) with 1.5 cm windows on the corners for imaging and additional lasers (figure 8). The MOT has three pairs of retro-reflected beams with a 15 mW cm^{-2} intensity, 6 cm $1/e^2$ diameter each and a typical detuning of 31 MHz. The capture velocity under equivalent conditions in rubidium is larger than 18 cm s^{-1} which gives a single pass trapping efficiency of 10^{-5} [58].

To improve over the single pass efficiency one needs to force the atoms to go through the trapping region several times. The dry film coating prevents the atoms from sticking to the walls, but the atoms can still escape through an exit hole. The new design maximized the number of bounces by eliminating the exit holes. The trap has an yttrium neutralizer foil ($1 \text{ cm} \times 1 \text{ cm} \times 0.011 \text{ mm}$), which has been shown to work reliably in the past, heated to 1000 K for 1 s. The trap works in a pulsed mode with the neutralizer in a rotation stage. After accumulation of francium in the neutralizer the rotation stage blocks the only hole to the glass cell. DC current is then applied to the neutralizer to release atomic francium into the glass cell. The pulsed mode has the additional advantage that the neutralizer is only hot for a small fraction of the time minimizing any possible damage to the vacuum or coating. A typical cycle consists of 20 s of accumulation and 1 s of release which translates in a duty cycle loss of only 5%. Keeping the glass cell hole open most of the time increased the pumping speed and improved the vacuum. Once the atoms are trapped and the neutralizer removed, the atoms can be transferred through the lower hole into another chamber for further experiments. The efficiency from production to trapping is better than 2% [58] which corresponds to an improvement of more than a factor of 100 over the previous design. Similar studies have been performed for other alkali atoms [61, 62].

Table 1. Trapping efficiency of different groups.

Group (atom)	Efficiency (%)			
	Transport	Neutralizer	Optical	Total
Boulder (Fr) [35]	0.7		56	0.4
Legnaro (Fr) [53]	>50			
TRIUMF (K) [61]				0.06
Los Alamos (Rb) [63]		30	0.3	0.09
Los Alamos (Cs) [62]	>95	45	3	1.4
Stony Brook (Fr) [58]	>90	52	3.4	2.0

2.3. Trapping efficiency for radioactive atoms

The efficiency can be decomposed into two contributions: the transfer efficiency from production to the vapour cell and the optical trapping efficiency. The Boulder group uses a decay source, and the transport efficiency includes the extraction from the oven and introduction into the vapour cell. They achieved an overall francium trapping efficiency of 0.4% [35]. Other groups use atoms implanted in a target. The transfer efficiency includes the extraction, transport and neutralization efficiency in this case. The first one describes the ionization and extraction of the atoms from the target. The second one gives the electrostatic transport efficiency from the target to the neutralizer. The last one is the release of neutral atoms from the neutralizer into the vapour cell. Table 1 shows the trapping efficiency obtained by different groups. The extraction efficiency for target experiments is not included. The Legnaro group is still optimizing its system which has a transport efficiency better than 50% [53]. The TRIUMF group has reported a total efficiency of 0.06% [61]. The rubidium trapping efficiency of the Los Alamos group is 0.09% [63], and they have improved it considerably for their caesium trap to reach 1.4% [62]. The second generation Stony Brook system [58] has reached a francium trapping efficiency of 2.0%. The improvement from the value previously reported comes from a detailed study of the losses due to aberrations in their imaging system that caused them to underestimate the number of trapped atoms.

3. Spectroscopy of Fr

Atomic properties are sensitive to different ranges of the electron wave function. Measurements of the location of energy levels, hyperfine splittings and atomic lifetimes are fundamental for understanding the atom quantitatively. The comparison between the state-of-the-art theoretical *ab initio* calculations and experiment tests the theoretical ability to predict a complicated atom and permits refinement of the calculational methods necessary for atomic PNC. The energy levels are the direct eigenvalues of the wave functions, but do not give detailed information about the r dependence of the wave function in a particular range. The radiative lifetime, τ , depends on the matrix element of the dipole moment operator, $e\mathbf{r}$, spatially integrated with the wave functions of the two connected levels. It is most sensitive to large r properties, while the hyperfine interaction probes the wave functions at the nucleus ($r \approx 0$).

A stringent test of atomic theory is the calculation of the lifetime of an electronic state. The calculation relies on having very good wave functions for all the levels involved. The lifetime τ of an excited state is determined by its individual decay rates, $1/\tau_i$, through the matrix element associated with the i th partial decay rate. The connections between lifetime, partial decay

rates and matrix elements are

$$\frac{1}{\tau} = \sum_i \frac{1}{\tau_i}, \quad (1)$$

$$\frac{1}{\tau_i} = \frac{4}{3} \frac{\omega^3}{c^2} \alpha \frac{|\langle J \| r \| J' \rangle|^2}{2J' + 1}, \quad (2)$$

where ω is the transition frequency, c is the speed of light, α is the fine-structure constant, J' and J are respectively, the initial and final state angular momenta and $|\langle J \| r \| J' \rangle|$ is the reduced matrix element [32]. Equation (2) links the lifetime of an excited state to the electronic wave functions of the atom. The comparisons of measurements with theoretical predictions test the quality of the computed wave functions especially at large distances from the nucleus due to the presence of the radial operator.

3.1. Experiments

The Boulder group used their francium MOT to perform measurements on the 7p levels of ^{221}Fr while the Stony Brook group has studied the spectroscopy of francium in a MOT on-line with an accelerator. The captured atoms are confined for long periods of time in a small volume moving at low velocity, an ideal environment for precision spectroscopy. The Stony Brook investigations includes the location of the 8s, 9s and 7d energy levels. The 8s energy level, not observed before, is a prime candidate for use in a PNC experiment. A set of measurements of radiative lifetimes includes the 7p, 8p, 8s, 9s and 7d levels in francium. The measurement of the hyperfine splitting of the $7P_{1/2}$ level in a series of isotopes was used to extract information on the nuclear magnetization through the Bohr Weisskopf effect [64] (hyperfine anomaly). The precision achieved in lifetime measurements of the $7P_{1/2}$ and $7P_{3/2}$ levels is comparable to that achieved in stable atoms and permits direct comparison with *ab initio* calculations of the appropriate matrix elements. The measurements on the 7d levels help extend the knowledge of this class of atomic wave functions in which correlation effects are very significant. The measurements test atomic theory in a heavy atom where relativistic and correlation effects are large.

3.1.1. Energy levels. The work on francium at ISOLDE located many of the energy levels and measured their hyperfine splittings [38]. The nuclear structure parameters extracted from these measurements have been very valuable. The short interaction time available at ISOLDE limited significantly the possible manipulation of the states. The long interaction times achievable in a MOT facilitate the study of the low lying levels in francium by multiphoton excitation. Tables 7 and 8 in the appendix contain an extended summary of the energy levels measured in Fr.

The approach to find an energy level requires the preparation of a cold sample of atoms in a MOT. Then it is necessary to find the appropriate path to reach the level. To measure the location of a level it is necessary to find a clean signature that is identifiable from the background. The signatures can be changes in the MOT fluorescence when the atoms are excited to another state, fluorescence at a very different energy than that used to excite the atom as it decays down to the ground state or even delayed fluorescence at the same excitation energy. Each one of these methods has advantages and disadvantages, and it is common to use them in combination with lock-in detection. The measurement usually requires very strong background rejection. Calibrated wavemeters allow simultaneous record of the energy of the exciting light with the fluorescence signal, but the iodine molecule atlas [54] has also been used for this purpose.

Theoretical calculations can guide the search for an excited state. *Ab initio* energy level calculations have expected accuracies of about 25 cm^{-1} which makes for a very large frequency

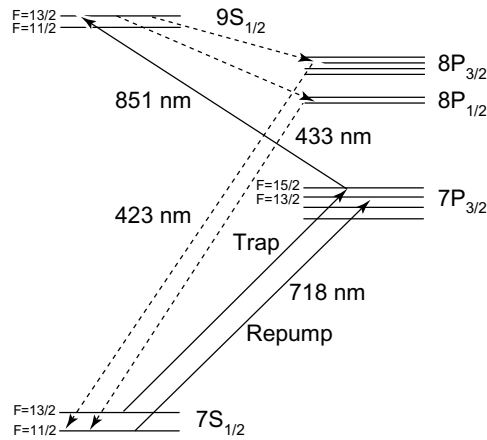


Figure 9. Diagram of energy levels of ^{210}Fr relevant for trapping and two-photon excitation of the 9s level (figure from [26]).

scan. However, once some levels with the same angular momentum have been measured, as is the case for the s and d series in francium [38, 40], a quantum defect fit can make predictions that reach accuracies of 1 cm^{-1} . The quantum defect is a semi-empirical approach to predicting energy levels. It assumes that the levels follow the Rydberg formula, but the principal quantum number may be different, by the quantum defect, from the appropriate integer. The paper by Drake and Swainson [65] explains the method and the physical interpretation of the different approximations.

When using a MOT for spectroscopic measurements it is important to consider the Autler–Townes splitting [66] of the excited states because of the presence of the strong laser that does the trapping and cooling. This splitting opens two possible avenues of excitation only a few megahertz apart.

9s level. Figure 9 shows the relevant levels necessary for excitation and detection of the 9s level [26]. The Stony Brook group used a quantum defect fit to narrow their search. They excited the atoms via a two step process ($7S_{1/2} \rightarrow 7P_{3/2} \rightarrow 9S_{1/2}$). The trapping laser provided the first photon and a narrow-linewidth diode laser operating at 851 nm provided the second. To locate the resonance a very clear signature, independent of background, came from blue photons at 433 and 423 nm as the atom decayed from the 9s state via the $8P_{3/2}$ and $8P_{1/2}$ levels. A photon counting system detected the blue photons. The fluorescence coming from the cycling transition of the trap showed a strong correlation with the blue photon signal as the population decreased when the second step excitation hit resonance. The two signals showed the asymmetries expected from the Autler–Townes splitting of the $7P_{3/2}$ [67]. Figure 10 shows the resonance detected in the count of blue photons as a function of the second step (851 nm) laser frequency. The energy difference between the $9S_{1/2}$ level and the $7S_{1/2}$ ground state is $25\,671.021 \pm 0.006\text{ cm}^{-1}$. The uncertainty was dominated by the absolute calibration of the I_2 atlas and the wavemeter.

8s level. The location of the 8s followed a similar technique to that of the 9s. It started with a quantum defect calculation that included the measured value for the 9s level, and used a similar technique: two step excitation from the $7S_{1/2} \rightarrow 7P_{3/2} \rightarrow 8S_{1/2}$.

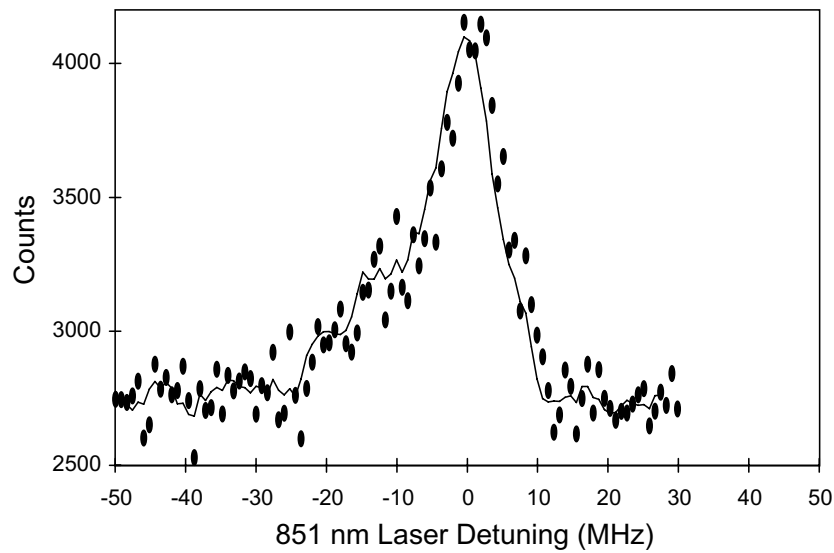


Figure 10. Blue photons from the 9s resonance of Fr as a function of the 851 nm laser. The zero of the scan corresponds to $11\,746.978 \pm 0.003 \text{ cm}^{-1}$. The continuous line is a running average to guide the eye (figure adapted from [26]).

The Stony Brook group used two different levels, $7P_{3/2}$ or $7P_{1/2}$, for the first step to the $8S_{1/2}$ level (see figure 4). Only the $8S_{1/2}$, $F = 13/2$ can be reached with an electric dipole allowed transition when the $7P_{3/2}$, $F = 15/2$ is the intermediate level. A $1.7 \mu\text{m}$ laser could excite this transition. Both the $8S_{1/2}$ hyperfine states can be reached when the $7P_{1/2}$, $F = 13/2$ is the intermediate state. A $1.3 \mu\text{m}$ laser could excite these transitions. The excitation with the $1.7 \mu\text{m}$ laser allowed detection of the resonance in two different ways. Observation of photons at 817 nm indicated that the atom decayed from the 8s state via the $7P_{1/2}$ levels, and a decrease in the cycling transition fluorescence indicated that some fraction of the population had been transferred to the $8S_{1/2}$ level.

The centre of gravity energy difference between the $7S_{1/2}$ ground level and the $8S_{1/2}$ level is $19\,732.523 \pm 0.004 \text{ cm}^{-1}$. The hyperfine separation of the $8S_{1/2}$, $F = 11/2$ and $F = 13/2$ states is $10\,256 \pm 7 \text{ MHz}$ giving a magnetic dipole hyperfine constant A of $1577.8 \pm 1.1 \text{ MHz}$ [27]. The uncertainty in these measurements was dominated by the accuracy of the wavemeter.

7d levels. Figure 11 shows a schematic of the apparatus for the study of the 7d levels. The Stony Brook group used very similar techniques as with the s states both for the estimation of their energy, quantum defect fits, and for their observations, double optical resonance spectroscopy.

They found the $7D_{3/2}$ and $7D_{5/2}$ levels with a sample of ^{210}Fr atoms confined and cooled in a MOT. The upper state of the $7P_{3/2}$ trapping transition serving as the resonant intermediate level to reach the 7d states.

The main limitations on the signal to noise ratio of the fluorescence were the quantum efficiency of the PMTs and background light from the hot neutralizer and the other lasers. These effects were greatest for the $7D_{5/2}$ level scans as the detection happened at 961 nm.

No correlations were found between the measured hyperfine splitting and the probe power, the trap laser power, the trap laser detuning, the Autler–Townes splitting or the direction of

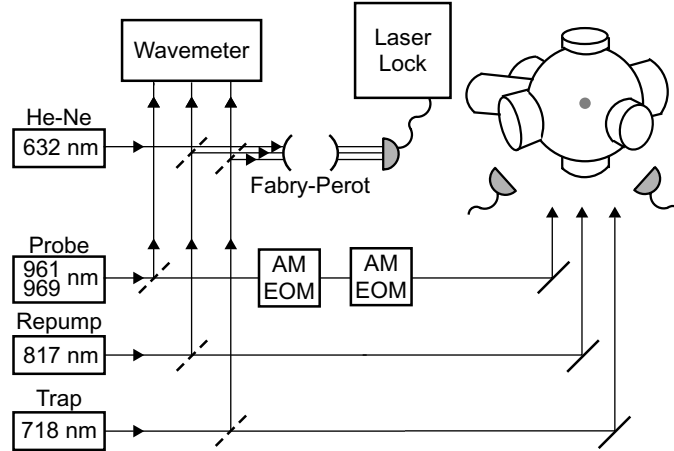


Figure 11. Block diagram of the apparatus for the measurement of the location of the 7d levels. The probe lite is amplitude modulated (AM) with two electro-optic modulators (EOM) in tandem (figure from [29]).

Table 2. Hyperfine splittings, hyperfine constants and energies from the ground state of the 7d levels of ^{210}Fr . Grossman *et al* [29].

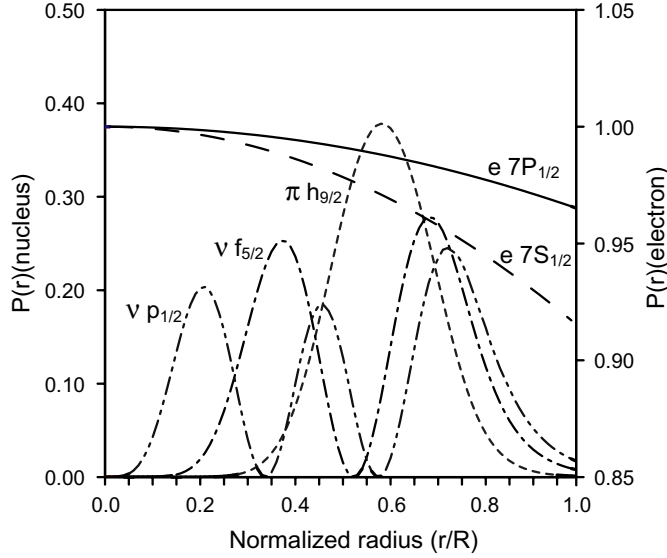
$\Delta(7D_{3/2}, F = 15/2 \leftrightarrow 13/2)$	$167 \pm 4 \text{ MHz}$
$\Delta(7D_{5/2}, F = 17/2 \leftrightarrow 15/2)$	$-117.5 \pm 2.5 \text{ MHz}$
$A(7D_{3/2})$	$22.3 \pm 0.5 \text{ MHz}$
$B(7D_{3/2})$	0 (assumed)
$A(7D_{5/2})$	$-17.8 \pm 0.8 \text{ MHz}$
$B(7D_{5/2})$	$64.0 \pm 17.0 \text{ MHz}$
Energy($7D_{3/2}$)	$24\,244.831 \pm 0.003 \text{ cm}^{-1}$
Energy($7D_{5/2}$)	$24\,333.298 \pm 0.003 \text{ cm}^{-1}$
$\Delta E_{\text{fine}}(7d)$	$88.467 \pm 0.004 \text{ cm}^{-1}$

the probe scan. The results are summarized in table 2. To obtain the centre of gravity for the energy from the ground state they assumed $B(7D_{3/2}) = 0$ and extrapolated the energies of the inaccessible hyperfine levels from the hyperfine constants. The uncertainties in the hyperfine constants were dominated by statistics, while the calibration of the wavemeter dominated the uncertainty in the location of the centre of gravity of the transition energy.

3.1.2. ^{221}Fr 7p levels. The Wieman group has made spectroscopic measurements on ^{221}Fr in their apparatus. In the thermal vapour, they measured the hyperfine splittings of the $7P_{3/2}$ and $7P_{1/2}$ levels. They observed the individual hyperfine transitions by scanning the 718 nm laser, while the 817 nm laser was set (to either the $F = 2 \rightarrow F' = 3$ or $F = 2 \rightarrow F' = 2$ transition) to select one velocity group of atoms. They obtained the splittings by measuring the frequency differences between each hyperfine line using a high-resolution λ metre (accuracy of 3 MHz for small differences and 50 MHz for absolute frequency checked against the I_2 Atlas [54]). They also measured the absolute values of the D_1 and D_2 lines. The uncertainties in the hyperfine constants A and B are better than previously published numbers [40, 68] by more than a factor of three. Table 3 presents a summary of their measurements. The uncertainty is dominated by the accuracy of their wavemeter.

Table 3. Hyperfine constants and wave numbers of the 7p level of ^{221}Fr . Lu *et al* [35].

$A(7P_{3/2})$	$66.5 \pm 0.9 \text{ MHz}$
$B(7P_{3/2})$	$-260 \pm 4.8 \text{ MHz}$
$A(7P_{1/2})$	$811.0 \pm 1.3 \text{ MHz}$
Energy($7P_{1/2}$)	$12\,236.6579 \pm 0.0017 \text{ cm}^{-1}$
Energy($7P_{3/2}$)	$13\,923.2041 \pm 0.0017 \text{ cm}^{-1}$

**Figure 12.** Simplified diagram of the origin of the hyperfine anomaly. Model wave functions in the nucleus of neutrons (ν), the last unpaired proton (π) and $S_{1/2}$ and $P_{1/2}$ electrons as a function of normalized nucleus radius. The nucleon probability densities should be read from the left axis and the electron probability densities from the right axis. The electron probability densities have been normalized to be 1 at $r/R = 0$.

3.1.3. Hyperfine anomaly. The hyperfine interaction between the magnetic field from the electron orbital and the nuclear magnetic moment should be proportional to the nuclear moment for different isotopes. However, due to the finite size of the nucleus there are small changes between different isotopes that perturb the size of the interaction by what is called the hyperfine anomaly (Bohr Weisskopf effect [64]). Although there is much information about the distribution of protons within the atomic nucleus, very little is known about the distribution of neutrons in nuclei, and it is necessary to rely heavily on theory. A unique experimental probe of the nuclear magnetization distribution is precision measurements of the magnetic hyperfine constants (A) with laser spectroscopy. The magnetic hyperfine interaction can be viewed as arising from an effective magnetic field by the electron interacting with the magnetization of the nucleus (see figure 12). Different atomic states have different radial wave functions and will sample the nuclear magnetization distribution with different weighting. The nuclear wave functions in figure 12 are from [69, 70] while the electronic wave functions are from [64]. A possible way to get at the neutron positions in the nuclei is to look at the radial dependence of the magnetization generated by the neutrons.

The Stony Brook measurements of the hyperfine structure of the $7P_{1/2}$ level for $^{208-212}\text{Fr}$ have a precision of 300 ppm [28, 71]. These measurements along with previous ground

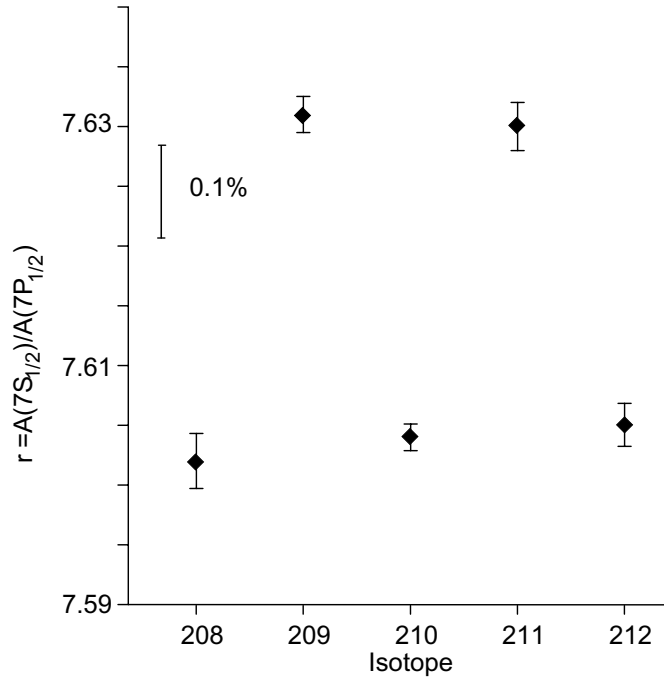


Figure 13. Ratio of hyperfine A magnetic dipole constants of $7S_{1/2}$ and $7P_{1/2}$ states observed for five different Fr isotopes. The s states come from the work of Coc *et al* [39] and the p states come from [28].

state hyperfine structure measurements reveal a hyperfine anomaly from the Bohr Weisskopf effect [64].

To obtain a high signal to noise ratio out of the few thousand trapped atoms, the Stony Brook group excited the atoms to the appropriate hyperfine state and used photon counting techniques. To avoid systematic errors in the calibration of a frequency marker as well as possible slow shifts (tens of minutes) in the laser frequency, they FM the probe laser to generate sidebands separated at about the hyperfine splitting of the $7P_{1/2}$ level (≈ 6 GHz).

Figure 13 shows the ratios of the $7S_{1/2}$ to $7P_{1/2}$ hyperfine A constants for a series of isotopes of Fr. There is a distinctive even–odd alternation well beyond the size of the error bars. The qualitative explanation of this observation requires the use of proton and neutron radial distributions as those from figure 12, and the agreement between theory and experiment is better than 1% (see [28]).

3.1.4. Lifetime measurements. There has been considerable interest in measuring radiative lifetimes of the alkali lowest atomic levels to test the *ab initio* calculations. A result of the activity is the resolution of a prior discrepancy between the theoretical and experimental lifetimes in Li [72] and Na [73–75]. Recent measurements are now in agreement with the calculations. The case of caesium is particularly important. The D_2 line lifetime has been under intensive work both experimentally [76–78] and theoretically [17, 18, 79]. The results bring credibility to the atomic calculations and strengthen the knowledge of the atom. Table 6 in the appendix summarizes the results of the electronic lifetimes measured in francium to date.

The most intuitive way to measure an atomic lifetime is to excite the atoms and record the exponential decay of the fluorescence as a function of time. It is important to have a quantitative understanding of the measurement equipment. To measure a time interval, the time scale must be precisely calibrated.

In time-correlated single-photon counting a laser repetitively excites the atoms and a fixed position detector collects the fluorescence as a function of time [80]. The atoms move slowly so that the solid-angle for the fluorescence collection is constant. The method relies on fast electronics to precisely record the time interval for detection events. Count rates are low to prevent the dead-time effects in the electronics and the preferential counting of early events. Low particle densities are necessary to minimize radiation trapping and quenching effects due to collisions. Advantages of the method include good statistics and less sensitivity to the divergence of the atomic source.

The Stony Brook approach to measure lifetimes utilized the limited number of available ^{210}Fr efficiently. The preparation of the state to measure required moving population with depumping and repumping pulses. Their order and intensity can be critical for the success of the measurement. The rejection of background light needed careful timing, interference filters and good imaging. When fast pulses were not available, it was necessary to deconvolve the full excitation function for the extraction of the lifetime.

All data were first corrected for pulse pile-up to compensate the fact that the early events are preferentially counted [80]. Then the data were fit to the appropriate decaying function. The results of fits can show sensitivity to the beginning or ending position of the sample causing a so-called truncation error [77].

Among the systematic effects that may be present in lifetime measurements performed in a MOT are hyperfine and Zeeman quantum beats. Their presence, even when small, could modify the result slightly. It is possible to bound their size using a worst case scenario considering the maximum magnetic field present. All the lifetime measurements performed at Stony Brook have such a contribution to the error budget.

7p levels. Two electro-optic modulators (EOM) turned off the trapping laser at 718 nm which provided the excitation for the $7P_{3/2}$ lifetime measurement. The 718 nm trapping laser was on continuously for the $7P_{1/2}$ measurement. A second laser at 817 nm repumped the atoms on the $7S_{1/2}, F = 11/2 \rightarrow 7P_{1/2}, F = 13/2$ transition. The repumping laser, chopped with the EOMs, provided the excitation for the $7P_{1/2}$ lifetime measurement. The lifetime measurement of the $7P_{1/2}$ level required a way to actively transfer population (depumper laser) from the $F = 13/2$ state to the $F = 11/2$ of the $7S_{1/2}$ ground state. See figure 14 for a diagram of the timing sequences for the two measurements.

A data set consisted of $\approx 1 \times 10^5$ fluorescence counts/channel accumulated with atoms in the trap in about 20 min (see figure 15(a)). A background count was taken for the same length of time with the trapping laser frequency off resonance so that there were no atoms in the trap. The background data set gave the excitation function for the atoms (see figure 15(b)). In case there was background from the radiation associated with the nuclear reaction, the 100 MeV ^{18}O beam was on the target while accumulating the signal and background data set. The subtraction of the background from the signal sets gave the data which is the exponential decay of the fluorescence for ≈ 5 lifetimes (see figure 15(c)).

The number of atoms in the trap was small ($N \approx 1000$), and the typical diameter of the trap was ≤ 1 mm. This minimized the possibility of multiple absorption. The unobserved contribution of Zeeman quantum beats could at most contribute by 0.01% to the total lifetime.

To search for other possible shifts in the lifetime, the Stony Brook group measured the lifetime of the $5P_{3/2}$ level of ^{87}Rb using exactly the same apparatus and technique. With Rb in

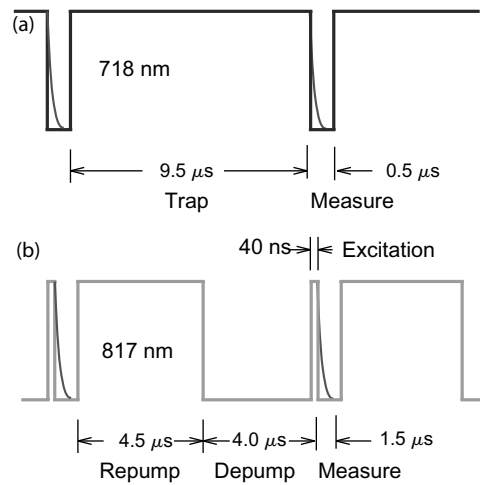


Figure 14. Timing for the lifetime measurements: (a) for D_2 line and (b) for D_1 line.

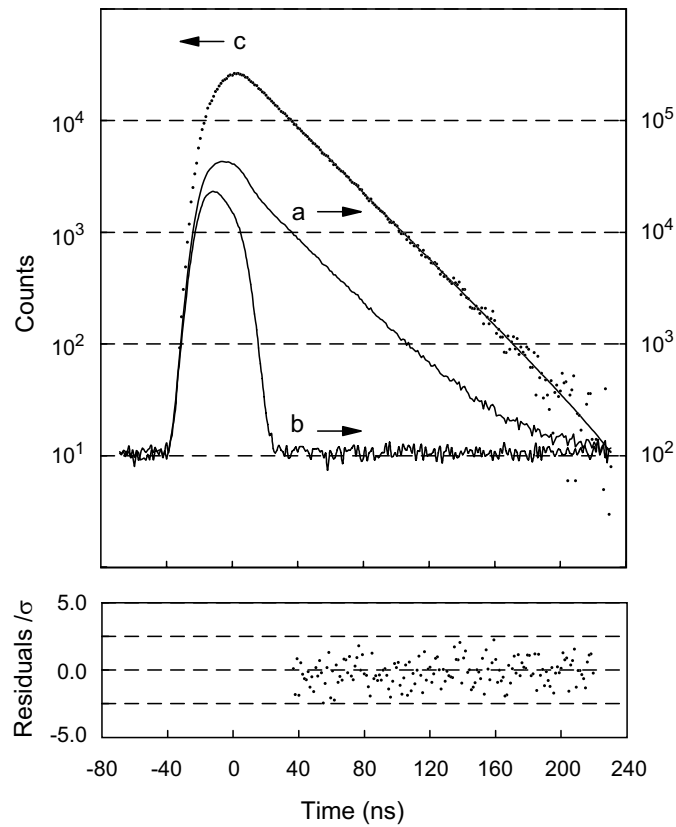


Figure 15. Decay curves of the $7P_{1/2}$ level of Fr. Trace a is the raw data with Fr in the trap and trace b is the background. Trace c is the subtraction of a minus b, and the straight line is a pure exponential fit to trace c. The bottom shows the residuals of the fit divided by the statistical uncertainty of each point. The reduced $\chi^2 = 0.98$ (figure from [31]).

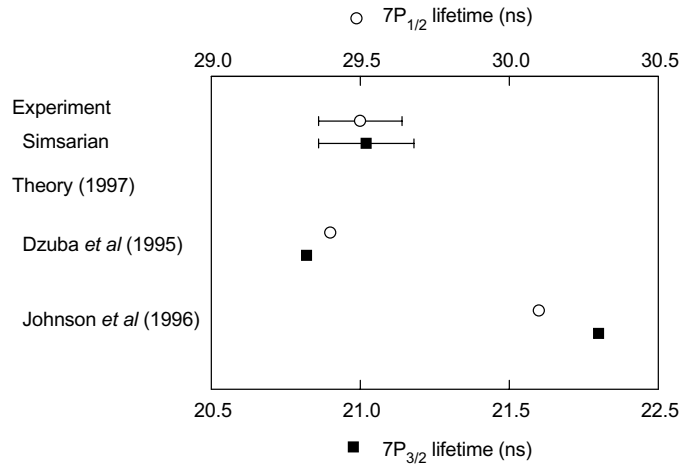


Figure 16. 7p lifetimes of Fr. Experiments and theory (figure from [31]).

the trap, it was possible to vary the number of atoms by decreasing the repumper power. The position of the trap was changed by one trap diameter, and the magnetic field gradient varied by 50% up and down from the value used with Fr. For all these tests no appreciable effect was found within the statistical error of the lifetime from a single data run. This number was taken as a limit on other systematic errors. The final errors in the lifetime measurements on the 7p level were dominated by the truncation error in the 7P_{3/2} level and the systematic errors for the 7P_{1/2} level.

Figure 16 shows the lifetime results of the 7p level in Fr and a comparison with the calculated lifetimes. Using the experimentally measured transition energies, equation (2), and the 21.02 ± 0.15 ns (29.45 ± 0.11 ns) lifetimes, they obtained reduced matrix elements of $5.898 \pm 0.022 a_\infty$ ($4.277 \pm 0.008 a_\infty$) in atomic units for the $7S_{1/2} \rightarrow 7P_{3/2}$ ($7S_{1/2} \rightarrow 7P_{1/2}$) transitions, with a_∞ the Bohr radius [30, 31].

From the two measurements of the lifetimes of the 7p levels it is possible to extract the atomic line strength ratio. This reveals the large relativistic effects in the heavy Fr atom. The line strength ratio, $S_{1/2}/S_{3/2}$, is the ratio of the reduced matrix elements squared and is independent of the transition energies. For the non-relativistic case of the light alkali elements the ratio is 0.5. As the relativistic effects become more important in heavier elements the ratio increases. Figure 17 plots the line strength ratio for the alkali. The Stony Brook result of 0.526(3) for $S_{1/2}/S_{3/2}$ in Fr shows a dramatic increase in relativistic effects over Cs that helps in the expected size of the observable atomic PNC. The values of the line strength ratio other than for Fr come from [74, 81, 82].

7d levels. The upper state of the 7P_{3/2} trapping transition served as the resonant intermediate level for the two-step excitation of the 7d states [32]. A probe laser provided the second step of the excitation, and the lifetime measurement came from the detection of the decay of the atomic fluorescence. The measured lifetimes are 73.6 ± 0.3 ns and 67.7 ± 2.9 ns for the 7D_{3/2} and 7D_{5/2} levels, respectively. The total errors are dominated by the statistical error. Table 4 shows a comparison with different theoretical predictions *ab initio* [79, 83] and semi-empirical calculations [84–86] of the lifetime measurements of the 7d levels [32].

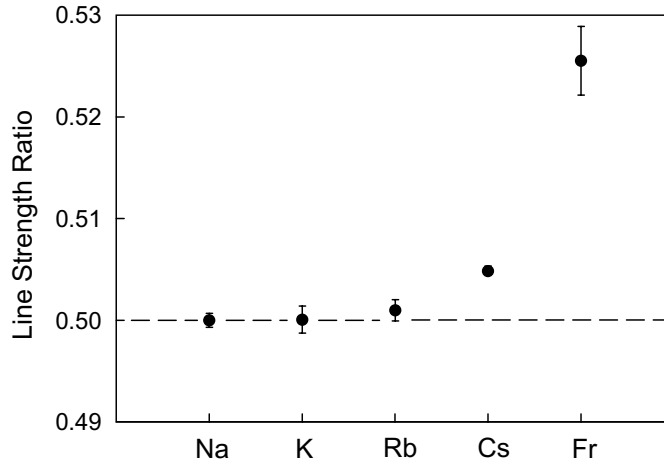


Figure 17. Ratio of line strength of the lowest P levels for alkali atoms. Deviations from 0.5 indicate relativistic effects (figure adapted from [31]).

Table 4. Comparison of measured lifetimes with theoretical predictions from semi-empirical and *ab initio* calculations of radial matrix elements.

	$\tau(7D_{3/2})$ (ns)	$\tau(7D_{5/2})$ (ns)
Grossman <i>et al</i> [32] ($\tau(7D_J)$)	73.6 ± 0.3	67.7 ± 2.9
Dzuba <i>et al</i> [83]	75.4	68.7
Safronova <i>et al</i> [79]	76.0	69.5
van Wijngaarden and Xia [84]	75.9	70.3
Biémont <i>et al</i> [85]	53	77
Theodosiou [86]	74.5	82.7

8s level. The 8s level in francium is particularly important because it corresponds to the level used in caesium for optical PNC measurements [10, 87]. Figure 18 shows the relevant levels and lasers used by the Stony Brook group for the measurement [34]. They excited the atoms to the 8s level with a two-step dipole transition. A 817 nm laser took the atoms to the $7P_{1/2}$ level and a $1.3 \mu\text{m}$ laser completed the two photon excitation. The excited atoms could decay back to the ground state through two different decay channels. The first channel used the same levels as the excitation lasers. The second channel went through the $7P_{3/2}$ level, and they detected the 718 nm photon coming from the last step of this decay. They obtained the lifetime of the 8s level using the decay signal and the previously measured lifetime of the $7P_{3/2}$ level [31]. The uncertainty in the lifetime of the $7P_{3/2}$ level propagates to the 8s level giving a Bayesian error of 0.15%.

The study of systematic effects was complemented with the equivalent level (6s) in rubidium where they measured the lifetime using two different atom sources: a MOT and a vapour cell [88]. The agreement on the measurement with two systems subject to different systematic effects reinforces the understanding of the results. They found a lifetime of the 8s level of 53.30 ± 0.44 ns [34]. The $\pm 0.82\%$ error in the measurement was dominated by statistical error. Figure 19 shows a comparison of the experimental result with different theoretical predictions, some *ab initio* and others semi-empirical.

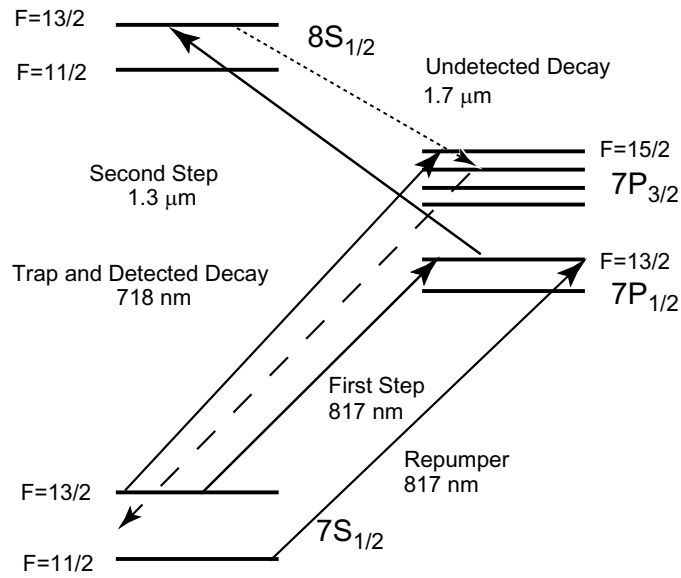


Figure 18. Energy levels of ^{210}Fr . The figure shows the trapping and repumping transitions (—), the two-step excitation (—), the fluorescence detection used in the lifetime measurement (- - -) and the undetected fluorescence (· · · · ·).

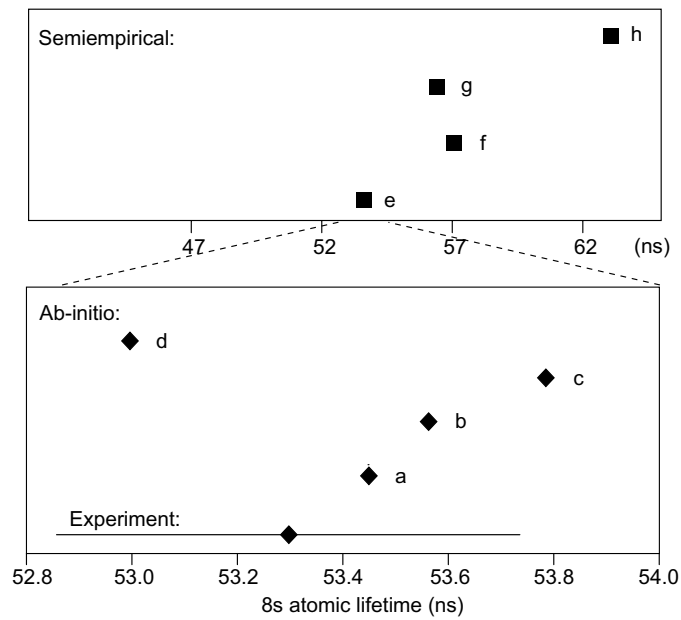


Figure 19. Comparison of the $8s$ level lifetime with *ab initio* calculations: (a) [79], (b) [83], (c) [89] and (d) [90], and semi-empirical calculations: (e) [91], (f) [86], (g) [85] and (h) [84] (figure from [34]).

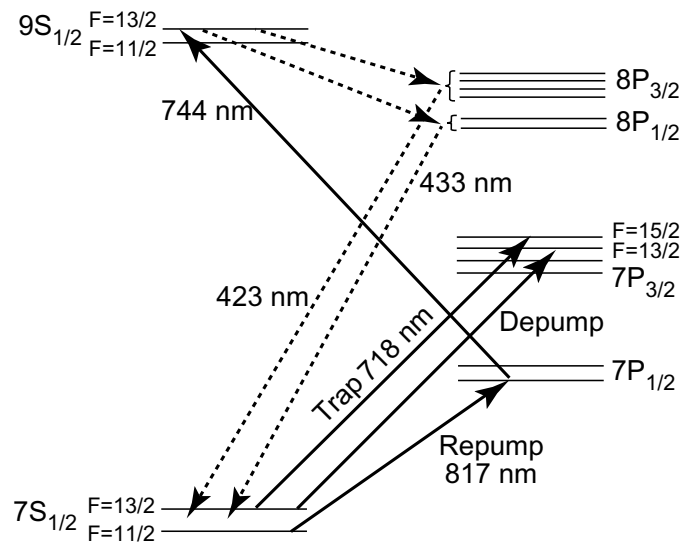


Figure 20. Energy levels and decay channels of ^{210}Fr involved in the decay of the 9s and 8p levels. The solid line arrows represent the excitation lasers relevant to the measurements of the $9S_{1/2}$, $8P_{3/2}$ and $8P_{1/2}$ lifetimes. The dashed line arrows represent the decay path used in the lifetime measurement of the 8p levels (figure from [92]).

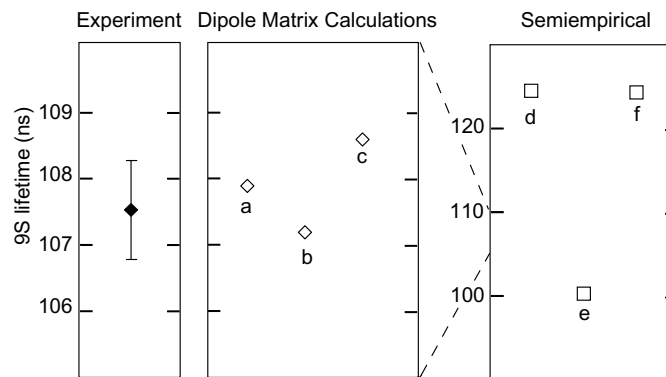


Figure 21. Comparison of the measured $9S_{1/2}$ level lifetime with theoretical predictions from radial matrix elements: (a) [79], (b) [94], (c) [91], and semi-empirical calculations: (d) [84], (e) [85], (f) [86] (figure from [33]).

9s level. The lifetime of the 9s level has been measured at Stony Brook with a two-step excitation [33, 92]. The repumper laser at 817 nm took the atoms to the $7P_{1/2}$ level and a 744 nm laser completed the transition after appropriate transfer of population to the lower hyperfine level of the 7s manifold. Rapid modulation of the intensity with a combination of acousto-optic and electro-optic modulators was followed by the detection of the fluorescence from the 9s level to the $7P_{3/2}$ level at 851 nm (figure 20).

The dominant uncertainty contribution is statistical. But there was an extensive search for other systematic effects both in Fr and with the equivalent (7s) level in Rb [93]. The lifetime of the 9s level is 107.53 ± 0.90 ns [33]. The theoretical predictions agree well with the experimental measurement as shown in figure 21.

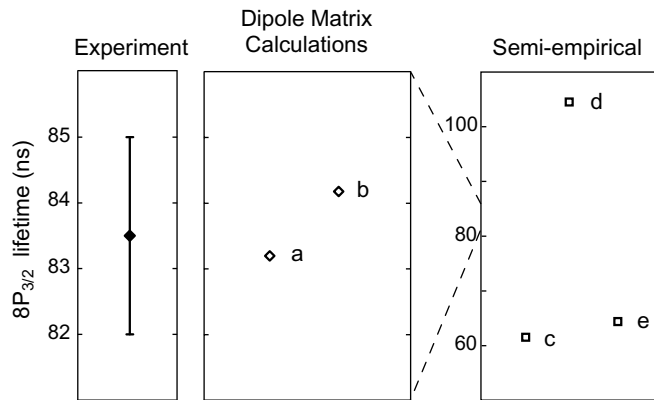


Figure 22. Comparison of the measured $8P_{3/2}$ level lifetime with theoretical predictions from radial matrix elements: (a) [79], (b) [94], and semi-empirical calculations: (c) [84], (d) [85], (e) [86] (figure from [95]).

8p level. The $9s$ level can decay to the $8p$ levels and from there go to the ground state as shown in figure 20. The Stony Brook group has used this decay channel to obtain the lifetime of the $8p$ levels in a way similar to that used for the $8s$ level [34] described above. An atom decaying through the $8P_{1/2}$ ($8P_{3/2}$) level will emit a 433 (423) nm photon on its way to the ground state. They obtained the lifetime of the $8p$ levels by detecting this fluorescence and using the measured lifetime of the $9s$ level. The fine separation of the $8p$ levels in francium is sufficiently large that the fluorescence photons coming from each fine level could be resolved with the use of interference filters. This is not the case in rubidium where the separation is so small that both fine levels had to be considered together [93].

The uncertainty in the lifetime of the $9s$ level has to be propagated for the result on the $8p$ levels giving a Bayesian error of 1.44% for the $8P_{3/2}$ level and 0.44% for the $8P_{1/2}$ level. The uncertainty is dominated by statistics, both from the fit and from the Bayesian contribution. In order to improve the measurement using this method it is not enough to take more data; it is also necessary to reduce the uncertainty on the $9s$ level lifetime measurement.

The results of the measurements gave a lifetime of 83.5 ± 1.5 ns for the $8P_{3/2}$ level and 149.3 ± 3.5 ns for the $8P_{1/2}$ level. Figures 22 and 23 show comparisons of the experimental results with theoretical predictions.

3.2. Atomic structure of francium

The calculations of the Flambaum group of New South Wales [83, 90] and the Johnson group of Notre Dame [79, 89] agree well with the measurements testing their ability to generate appropriate Fr wave functions for many important energy levels for an atomic PNC measurement. They use many-body perturbation theory (MBPT) to calculate the atomic structure of francium to a high accuracy. To achieve precise results in the heavy alkali atoms, the interaction between the valence and the core electrons must be calculated. This is the most complicated part of the method. Two recent reviews of these methods include [6, 7].

Dzuba *et al* use MBPT to calculate $E1$ transition amplitudes in Fr. They begin with a relativistic Hartree–Fock (RHF) method to obtain a complete set of electron wave functions. They calculate the single-particle electron wave functions in the effective RHF potential as a perturbation expansion in terms of the difference between the exact and RHF Hamiltonians.

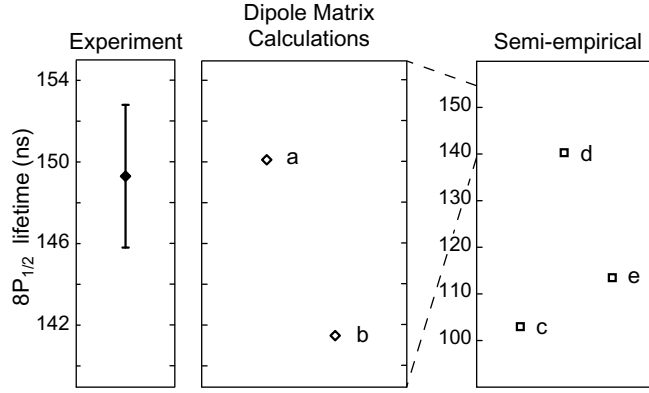


Figure 23. Comparison of the measured $8P_{1/2}$ level lifetime with theoretical predictions from radial matrix elements: (a) [79], (b) [90], and semi-empirical calculations: (c) [84], (d) [85], (e) [86] (figure from [95]).

The relativistic equations automatically take into account the spin–orbit interaction. The time-dependent Hartree–Fock (TDHF) method gives the polarization of the core by the optical field. This changes the radial integral by -7% .

They calculate the states for the electron outside the core with the single-particle equation using the Brueckner approximation:

$$(H_0 + \Sigma)\psi = E\psi, \quad (3)$$

where H_0 is the relativistic Hartree–Fock–Dirac Hamiltonian and Σ is the self-energy operator. The self-energy operator accounts for the correlation interaction of the valence electron with the core. Correlations arise from the Coulomb interaction between electrons in the many-body system. Dzuba *et al* [83] calculate lowest order contributions to Σ for Fr. They also consider two classes of higher-order correlations: the hole–particle interaction and the screening of the Coulomb interaction.

Once they determine Σ they find the states of the external electron by iteratively solving equation (3) starting with the RHF wave functions. This method accounts for the dominating Brueckner-type correlation diagrams that correct the radial integrals by $\approx -10\%$. The non-Brueckner correlations are mostly from structural radiation and renormalization of the wave function, that modify the radial integral by -0.4% . These are extrapolated from similar corrections in Cs. The accuracy of the calculated radial integrals in Fr by Dzuba *et al* is expected to be $\pm 1\%$. The RHF calculations of Johnson *et al* [79, 89] and Safronova are in good agreement with those of Dzuba *et al*.

The MBPT calculations predict the location of energy levels, hyperfine structure, $E1$ transition amplitudes and PNC transition amplitudes. These quantities are calculated from the MBPT atomic wave functions. Comparisons with experiments test the accuracy of the wave functions over different ranges of r .

The groups of Flambaum and Johnson have continued to refine their methods of calculation and have extended them to other energy levels outside the s and p manifolds [79, 90, 96]. A new generation of atomic structure calculations has been making rapid progress in this complex *ab initio* methodology; among many three have contributed directly or indirectly to atomic PNC in francium: Safronova at Delaware [96], Derevianko at Reno [23] and Koslov at St Petersburg [97]. At the same time other groups have fine-tuned their semi-empirical methods for the prediction of lifetimes, polarizabilities and other atomic properties [84–86, 91].

4. Parity non-conservation

PNC was measured for the first time in three experiments with weak charged currents in 1957 [98–100]. Attempts to unify the weak and electromagnetic interactions by Weinberg [101], Salam [102] and Glashow [103] showed the existence of a neutral heavy boson associated with the weak interaction. The effects of a neutral boson in atomic PNC had already been estimated years before by Zel'dovich [104]. The race for the detection of the consequences for nuclear currents started, and the high-energy community with the Gargamelle experiment at CERN saw a positive signature in the elastic muon–neutrino electron scattering [105]. The neutral weak interaction between the electron and the nucleons remained to be observed since it was dominated by the electromagnetic interaction. It was first observed in atomic PNC experiments [106–109] in 1978. Further experiments in high energy physics with inelastic scattering enhanced the evidence of the neutral electroweak interaction [110]. The particles responsible for the weak interaction (W^+ , W^- and Z^0) were observed in 1983 [111, 112].

Atomic PNC experiments, such as the Boulder one performed in caesium [113], measure an electric dipole transition rate between levels of the same parity. The extraction of weak interaction parameters from a PNC measurement requires the calculation of a matrix element that contains a weak interaction operator, energy levels coming from perturbation theory and polarizabilities (sums of electric dipole transition matrix elements). These quantities are sensitive to the electron wave functions at short, intermediate and large distances from the nucleus, respectively. The energy levels and electric dipole transition matrix elements can be measured directly from spectroscopy. Unfortunately, the weak interaction matrix element cannot be measured directly. Instead, in the Boulder caesium PNC experiment, what is measured is the product of the weak matrix element with the weak charge. Since the interest is in extracting the weak charge it is necessary to rely on a theoretical calculation of the weak matrix element. The short range weak interaction depends on the electron density at the nucleus.

The improvement in precision of the PNC measurement in caesium [10, 113] encouraged theorists to revisit their calculations to account for previously neglected corrections. The availability of high precision spectroscopic measurements made it possible to compare their predictions with measurements to below 1%. Several new corrections had to be included such as the Breit interaction [23], the strong-field radiative corrections [114, 115] and the self-energy and vertex contribution [116, 117]. The relevance of the corrections will be different depending on the atom, which is why measurements in francium are important not only for a future PNC measurement in francium but also as a cross check for calculations in caesium.

Atomic physics experiments benefit from the long interaction time between the electron and the nucleus compared with high energy collisions. In the latter, the interaction time is of the order of the transit time through the nucleus, whereas in atomic physics, where there is no decay of the nucleus, the time is limited by the coherence time that can be on the order of seconds [118]. The neutral interaction between an electron and a nucleon can be mediated by a photon if it is electromagnetic, by a Z^0 boson if it is weak according to the minimal standard model. Both the photon and Z^0 channels are comparable at high energy, while the Z^0 channel is suppressed at low energies by $q^2/M_{Z^0}^2$ with q the momentum transfer and M_{Z^0} the Z^0 boson mass [119]. The suppression appears because at low energies the interaction happens through virtual Z^0 bosons since there is not enough energy to create them. The experiments at low and high energies are sensitive to different quantities and become complementary. For example, electron scattering at the Z^0 pole can be used to obtain a value for the Weinberg angle, but if that value does not agree with the one extracted from atomic PNC measurements that could be an indication of physics beyond the Standard Model.

Peskin and Takeuchi introduced a parametrization of physics beyond the standard model in terms of two parameters S and T [120, 121]. Atomic PNC measurements are sensitive almost only to the S parameter and can be used in combination with other experiments to separate the S and the T contributions [7]. PNC measurements are particularly sensitive to extra Z bosons [119]. A crude estimate for the effect of an extra Z boson can be obtained from the suppression at low energies. In the case where the extra boson is identical to its lighter counterpart the correction at low energies would be proportional to $M_{Z^0}^2/M_{Z_\chi}^2$ with M_{Z_χ} the mass of the extra boson. Since the precision of PNC measurements is $\sim 1\%$ the crude estimate sets a lower bound on the mass of the extra boson of $M_{Z_\chi} > 10M_Z = 912$ GeV. A careful analysis gives a lower bound for extra Z bosons from the caesium PNC measurement of $M_{Z_\chi} > 750$ GeV [7] which is higher than the 600 GeV limit set by direct searches at the Tevatron [122] and a global analysis including the experiments at LEP [123].

4.1. Atomic PNC theoretical background

The exchange of weak neutral currents between electrons and nucleons constitutes the main source of parity violating atomic transitions. The currents are of two kinds, depending on whether the electron or the nucleon enters as the axial vector current. The Hamiltonian for an infinitely heavy nucleon without radiative corrections is [124]

$$H = \frac{G}{\sqrt{2}}(\kappa_{1i}\gamma_5 - \kappa_{\text{nsd},i}\boldsymbol{\sigma}_n \cdot \boldsymbol{\alpha})\delta(\mathbf{r}), \quad (4)$$

where $G = 10^{-5} m_p^{-2}$ is the Fermi constant, m_p is the proton mass, γ_5 and $\boldsymbol{\alpha}$ are Dirac matrices, $\boldsymbol{\sigma}_n$ are Pauli matrices and κ_{1i} and $\kappa_{\text{nsd},i}$ are constants of the interaction with $i = p, n$ for a proton or a neutron and nsd = nuclear spin dependent. The standard model tree level values (no loops included in the calculation) for these constants with $\kappa_{\text{nsd},i} = \kappa_{2i}$ are

$$\begin{aligned} \kappa_{1p} &= \frac{1}{2}(1 - 4\sin^2\theta_W), & \kappa_{1n} &= -\frac{1}{2}, \\ \kappa_{2p} &= -\kappa_{2n} = \kappa_2 = -\frac{1}{2}(1 - 4\sin^2\theta_W)\eta, \end{aligned} \quad (5)$$

with $\sin^2\theta_W \sim 0.23$ the Weinberg angle and $\eta = 1.25$. κ_{1i} (κ_{2i}) represents the coupling between nucleon and electron currents when the electron (nucleon) is the axial vector.

In an atom, the contribution from equation (4) for all the nucleons must be added. It is convenient to work in the shell model approximation with a single valence nucleon of unpaired spin (nsi = nuclear spin independent):

$$H_{\text{PNC}}^{\text{nsi}} = \frac{G}{\sqrt{2}} \frac{Q_W}{2} \gamma_5 \delta(\mathbf{r}). \quad (6)$$

This contribution is independent of the nuclear spin and is proportional to the weak charge

$$Q_W = 2(\kappa_{1p}Z + \kappa_{1n}N), \quad (7)$$

with N the number of neutrons. Because of the strong cancellation in κ_{1p} the standard model value for the weak charge is almost equal to $-N$. The theoretical uncertainty present in all the extractions of weak interaction parameters from atomic PNC comes from the calculation of the matrix element γ_5 as the experiment is not sensitive to the weak charge itself but to the product as equation (6) states.

Looking at this last Hamiltonian it is possible to follow more exactly the Z dependence of the interaction for an s state atom for which PNC mixes some p character into its ground s state. The s level wave function grows as $Z^{1/2}$, the derivative (the momentum) of the p level at the origin goes as $Z^{3/2}$ and $Q_W \approx -N \approx -Z$ gives an overall scaling for the weak matrix element of $Z^3 R$, with R a relativistic enhancement factor. The enhancement

can be understood in a simple picture of the momentum of the electron that approaches the nucleus with Z increases to relativistic velocities (see the book of Khriplovich for an extended explanation [124]). As an example, the PNC effect of the spin independent part should be 18 times larger in francium than in caesium according to the calculations of [83, 96].

The second term of equation (4) is nuclear spin dependent (nsd), and due to the pairing of nucleons its contribution has a weaker dependence on Z . The result after adding over all nucleons is [125]

$$H_{\text{PNC}}^{\text{nsd}} = \frac{G}{\sqrt{2}} \frac{KI \cdot \alpha}{I(I+1)} \kappa_{\text{nsd},i} \delta(\mathbf{r}), \quad (8)$$

where $K = (I+1/2)(-1)^{I+1/2-l}$, l is the valence nucleon orbital angular momentum and I is the nuclear spin. The terms proportional to the anomalous magnetic moment of the nucleons and the electrons have been neglected.

The interaction constant is given by [125]

$$\kappa_{\text{nsd},i} = \kappa_{a,i} - \frac{K-1/2}{K} \kappa_{2,i} + \frac{I+1}{K} \kappa_{Q_w}, \quad (9)$$

with $\kappa_{2,i}$ given by equation (5) corresponding to the tree level approximation, and we have two corrections, the effective constant of the anapole moment $\kappa_{a,i}$ and κ_{Q_w} that is generated by the nuclear spin independent part of the electron nucleon interaction together with the hyperfine interaction. Flambaum and Murray show that [125]

$$\begin{aligned} \kappa_{a,i} &= \frac{9}{10} g_i \frac{\alpha \mu_i}{m_p \tilde{r}_0} \mathcal{A}^{2/3}, \\ \kappa_{Q_w} &= -\frac{1}{3} Q_w \frac{\alpha \mu_N}{m_p \tilde{r}_0 \mathcal{A}} \mathcal{A}^{2/3}, \end{aligned} \quad (10)$$

where α is the fine structure constant, μ_i and μ_N are the magnetic moment of the external nucleon and of the nucleus, respectively, in nuclear magnetons, $\tilde{r}_0 = 1.2$ fm is the nucleon radius, $\mathcal{A} = Z+N$, and g_i gives the strength of the weak nucleon-nucleus potential with $g_p \sim 4$ for a proton and $0.2 < g_n < 1$ for a neutron [124]. The interaction is stronger in heavier atoms since both $\kappa_{a,i}$ and κ_{Q_w} scale as $\mathcal{A}^{2/3}$ ($Q_w/\mathcal{A} \sim 1/2$ in κ_{Q_w}). The anapole moment is the dominant contribution to the interaction in heavy atoms, for example in ^{209}Fr , $\kappa_{a,p}/\kappa_{Q_w} \simeq 15$, so it is safe to assume that $\kappa_{\text{nsd},i} = \kappa_{a,i}$. Arguments similar to the nuclear spin independent part give a scaling for the matrix element of the nuclear spin dependent part of $Z^{8/3}R$. The effect in francium in this case is 11 times larger than in caesium.

4.2. The anapole moment

The anapole moment of a nucleus is a PNC, time reversal conserving moment that arises from weak interactions between the nucleons (see the recent review by Haxton and Wieman [126]). It can be detected in a PNC electron–nucleus interaction and reveals itself in the spin dependent part of the PNC interaction. Wood *et al* [10, 113] measured the anapole moment of ^{133}Cs by extracting the dependence of atomic PNC on the hyperfine energy levels involved and consequently nuclear spin. The measurement shows that atomic PNC is a unique probe for neutral weak interactions inside the nucleus, which otherwise remain hidden by much larger electromagnetic charged currents [127].

The anapole moment is defined by (see [128])

$$\mathbf{a} = -\pi \int d^3r r^2 \mathbf{J}(\mathbf{r}), \quad (11)$$

with \mathbf{J} the electromagnetic current density. The anapole moment in francium arises mainly from the weak interaction between the valence nucleons and the core. It is possible to think of it as a weak radiative correction that is detectable only with an electromagnetic interaction. Flambaum *et al* [129], by including weak interactions between nucleons in their calculation of the nuclear current density, estimate the anapole moment from equation (11) for a single valence nucleon to be

$$\mathbf{a} = \frac{1}{e} \frac{G}{\sqrt{2}} \frac{K\mathbf{j}}{j(j+1)} \kappa_{a,i} = C_i^{\text{an}} \mathbf{j}, \quad (12)$$

where j is the nucleon angular momentum. These values correspond to the nuclear values for the case of a single valence nucleon. The calculation is based on the shell model for the nucleus, under the assumption of homogeneous nuclear density and a core with zero angular momentum leaving the valence nucleon carrying all the angular momentum.

4.3. Status of PNC measurements

The weak interaction in atoms induces a mixing of states of different parity, observable through PNC measurements. Transitions that were forbidden due to selection rules become allowed through the presence of the weak interaction. The transition amplitudes are generally small and an interference method is commonly used to measure them. A typical observable has the form

$$|A_{\text{PC}} + A_{\text{PNC}}|^2 = |A_{\text{PC}}|^2 + 2\text{Re}(A_{\text{PC}}A_{\text{PNC}}^*) + |A_{\text{PNC}}|^2, \quad (13)$$

where A_{PC} and A_{PNC} represent the parity conserving and PNC amplitudes. The second term on the right side corresponds to the interference term and can be isolated because it changes sign under a parity transformation. The last term is usually negligible.

All recent and on-going experiments in atomic PNC rely on the large heavy nucleus (large Z) enhancement factor proposed by Bouchiat and Bouchiat [9, 130, 131]. These experiments follow two main strategies (see recent review by M-A Bouchiat [132]). The first one is optical activity in an atomic vapour. The asymmetry introduced by PNC makes the atoms interact preferentially with right (or left) circularly polarized light. A linearly polarized light beam propagating through an atomic vapour experiences a rotation of the polarization plane analogous to the one observed in the Faraday effect except that in this case there is no magnetic field present. The measurement strategy uses interference with an allowed transition to enhance the small effect. The amount of rotation is related to the weak charge, which quantifies the effect of the weak force. The method has been applied to reach a precision of 2% in bismuth [13], 1.2% in lead [133, 134] and 1.2% in thallium [11].

The second strategy measures the excitation rate of a highly forbidden transition. The electric dipole transition between the 6s and 7s levels in caesium becomes allowed through the weak interaction. Interference between this transition and the one induced by the Stark effect due to the presence of a static electric field generates a signal proportional to the weak charge. The best atomic PNC measurement to date uses this method to reach a precision of 0.35% [10, 113]. The exquisite precision reached on the caesium experiment at Boulder allowed the extraction of the anapole moment from their measurement [10, 113]. The transition is dominated by the spin independent contribution, which is proportional to the weak charge. They observed a small difference on the signal depending on the hyperfine levels used for the transition. The difference corresponds to the spin dependent contribution which for caesium is dominated by the anapole moment. They extracted the spin dependent contribution with an accuracy of 14% giving the first measurement of an anapole moment.

Other methods have been proposed and some work is already on the way. The Bouchiat group in Paris has been working also on the highly forbidden 6s to 7s electric dipole transition in a caesium cell but detects the occurrence of the transition using stimulated emission rather than fluorescence [135]. The Budker group in Berkeley has been pursuing measurements in ytterbium, which has many stable isotopes available [14, 136]. There is an on-going experiment in the Fortson group in Seattle using a single barium (or alternatively radium) ion [127, 137]. The group of DeMille at Yale is planning to measure anapole moments by placing diatomic molecules in a strong magnetic field [138]. A collaboration in Russia wants to measure the anapole moment in a potassium cell [139]. The groups at Legnaro and Maryland–Stony Brook–Yale are working towards a PNC measurement using francium [53, 140]. This list is not intended to encompass all the efforts, but represents some of the groups interested in PNC at present.

5. Considerations for a PNC experiment in francium

In order to enhance the small PNC effect in francium it is necessary to perform a measurement based on an ‘electroweak interference’ between a weak-interaction amplitude F_{pnc} associated with a Z^0 exchange and a parity conserving electromagnetic amplitude F associated with photon exchanges [124]. The means of looking for such an effect consist in preparing a handed experiment, one that can be performed in either a right-handed or a left-handed configuration. One measures the transition rate in the two configurations. The results of the two experiments differ by the electroweak interference term. In terms of a right–left asymmetry

$$A_{\text{RL}} = 2 \frac{\text{Re}(F F_{\text{pnc}})}{|F^2 + F_{\text{pnc}}^2|}. \quad (14)$$

The electromagnetic amplitude is much larger than the weak-interaction amplitude, and the experiments are designed to make the argument of the numerator real to maximize the effect, so the right–left asymmetry is simply

$$A_{\text{RL}} = 2 \frac{F_{\text{pnc}}}{F}. \quad (15)$$

Typical numbers for the asymmetry from the caesium experiments are a few parts per million [113]. The difficulty of the experiment consists in discriminating the tiny parity violating interference against parity-conserving signals that are many orders of magnitude larger. Systematic errors come from an imperfect reversal of the handedness of the experiment and give false parity violating signals that need to be checked by consistency.

5.1. The optical experiment

So far, there has been no PNC measurement in neutral atoms performed utilizing the new technologies of laser cooling and trapping. In order to create a road map for an experiment one could assume a transition rate measurement following closely the technique used by the Boulder group in caesium [140]. Start with a Stark shift to induce a parity conserving amplitude between the 7s and 8s levels of francium (figure 4) and look how this electromagnetic term will interfere with the weak-interaction amplitude giving rise to a left–right asymmetry with respect to the system of coordinates defined by the static electric field \mathbf{E} , static magnetic field \mathbf{B} and the Poynting vector \mathbf{S} of the excitation field, such that the observable is proportional to $\mathbf{B} \cdot (\mathbf{S} \times \mathbf{E})$.

Francium atoms would accumulate in a MOT. Then, after further cooling to control their velocities, they would be transferred to another region where a dipole trap will keep them ready

for the measurement. The measurement would be performed by moving the dipole trap with the atoms into the mode of a high finesse interferometer tuned to the 7s to 8s transition in a region with a dc electric field present. If an atom gets excited it will decay via the 7p state, but could also be ionized. Optical pumping techniques allow one to recycle the atom that has performed the PNC transition many times enhancing the probability to detect the signature photon. Redundancy in the reversal of the coordinates would suppress systematic errors. There is a strong assumption implicit in this statement that needs to be thoroughly studied: the trap does not affect the measurement.

To estimate the requirements for a PNC measurement in francium it is good to take the Boulder Cs experiment as a guide (see paper by Wieman in [19]). The most important quantity to estimate is the signal to noise ratio since that will determine many of the requirements of the experiment.

The approach of Stark mixing works as an amplifier in the full sense of the word; it enlarges the signal, but it also brings noise. The Stark induced part of the signal in photons per second is given in equation (16); this signal will contribute the shot noise to the measurement,

$$S_{\text{stark}} = \frac{16\pi^3}{3h\epsilon_0\lambda^3} E^2 \beta^2 I_0 N. \quad (16)$$

While the PNC signal in photons per second is

$$S_{\text{pnc}} = \frac{16\pi^3}{3h\epsilon_0\lambda^3} 2E\beta \text{Im}(E_{\text{pnc}}) I_0 N, \quad (17)$$

where β is the vector Stark polarizability, E the dc electric field used for the Stark mixing interference, N the number of atoms in the interaction volume, λ the wavelength of the transition, $\text{Im}(E_{\text{pnc}})$ the PNC amplitude expressed as an equivalent electric field and I_0 the normalized (to atomic saturation) intensity of the excitation source. Assuming only shot noise as the dominant source of noise, the signal to noise ratio achieved in 1 s is

$$\frac{S_{\text{pnc}}}{N_{\text{oise}}} = 2 \left(\frac{16\pi^3}{3h\epsilon_0\lambda^3} \right)^{1/2} \text{Im}(E_{\text{pnc}}) \sqrt{I_0 N}. \quad (18)$$

For francium in the 7s to 8s state, the ratio becomes

$$\frac{S_{\text{pnc}}}{N_{\text{oise}}} = 7.9 \times 10^3 \text{Im}(E_{\text{pnc}}) \sqrt{I_0 N}. \quad (19)$$

This last expression gives a result in $(\sqrt{\text{Hz}})^{-1}$ when using atomic units for the PNC term. It illustrates where a future measurement with francium is stronger: the size of the effect. The calculated value from Dzuba *et al* [83] for $\text{Im}(E_{\text{pnc}})$ of 1.5×10^{-10} in atomic units is eighteen times larger than in caesium.

The ratio does not depend on the particular details of the interference experiment used; that is, the value of the vectorial Stark polarizability of the 7s \rightarrow 8s transition β or in the particular value of the dc electric field chosen E . These factors enter in the signal to noise ratio once the technical noise is considered.

The very high intensities available in a standing wave will exert a repelling force that will tend to move the cold atoms to a region of low intensity. The FM modulation at integers of the free spectral range of the cavity can create a slowly moving travelling envelope to solve this problem as already suggested by the Boulder group. Another possible complication is the ionization of the Fr atoms that have been excited by a second photon of 507 nm. The ionization potential is only 4.07 eV and two of those photons add to 4.89 eV. Taking a typical ionization cross section of 10^{-18} cm^2 and an intracavity intensity of 10^6 W cm^{-2} the resulting ionization rate could amount to 1/6 of the decay rate from the 8s to the 7p state.

As the measurement proceeds alternating periods of cooling and trapping with periods of excitation, each time there is excitation some of the atoms will be lost. A careful balance between intracavity power and signal loss will be needed to find the optimal operating point.

5.2. The anapole moment measurement

There is interest in measuring the anapole moment in francium. The UMD–Stony Brook–Yale group have proposed inducing electric dipole ($E1$) transitions between the hyperfine levels of the francium ground state [141]. The transition that is forbidden by the selection rules becomes allowed due to the weak interactions that create the anapole moment. The $E1$ transition amplitude is almost proportional to the anapole moment since it is the dominant process for heavy atoms. The measurement of the anapole moment should give information on the weak nucleon–nucleon interactions inside the nucleus. A measurement of the anapole moment in a chain of isotopes should provide information to separate the anapole moment due to the valence proton from that of the neutron. The constraints that could be obtained for the proton and the neutron weak anapole moments are almost orthogonal in the weak meson–nucleon coupling space.

The proposal by UMD-SB-Yale for a measurement of the nuclear anapole moment is by direct excitation of the microwave electric dipole ($E1$) transition between the ground hyperfine states of an alkali atom. The transition is parity forbidden but is allowed by the anapole induced mixing of opposite parity states. The general approach has been suggested and followed in the past [12, 142–145]. It is a modification of the suggestion of Fortson [127] for atomic PNC to use an ion placed at the anti-node of a standing optical wave. The proposal would place many trapped atoms at the anti-node of a standing microwave field of a Fabry–Perot resonator. The atoms should be well localized within the anti-node of the electric standing wave (microwave frequency $\nu_m \sim 45$ GHz and wavelength $\lambda_m \sim 6.6$ mm for francium). A blue detuned dipole trap would keep the atoms at the anti-node of the standing wave while minimizing the perturbation introduced by the confinement. The PNC signal would be amplified by interfering it with a parity allowed Raman transition in the presence of a static magnetic field.

The fields present would define the system of coordinates for the experiment. The observable would be given by $i(\mathbf{E}_M \times (\mathbf{E}_1 \times \mathbf{E}_2)) \cdot \mathbf{B}$, with \mathbf{E}_M the microwave electric field, \mathbf{E}_1 and \mathbf{E}_2 the Raman fields, \mathbf{B} the static magnetic field and the i is present in accordance with time reversal symmetry. For a projection noise limited measurement [146], that is noise coming from the collapse that distributes the atoms binomially between the two hyperfine levels that leads to an uncertainty in the measured excited state fraction, the signal to noise ratio is given by

$$\frac{S}{\mathcal{N}_p} = 2 \frac{A_{E1} t}{\hbar} \sqrt{N}, \quad (20)$$

with A_{E1} the $E1$ transition amplitude, t the excitation duration and N the number of atoms. The signal to noise ratio grows linearly with the excitation time t . The future experiment requires not only good statistics but also control over many possible systematic effects [141].

A measurement of the anapole moment in Fr by direct $E1$ hyperfine transitions will require a big effort not only from the experimental side but also from the theoretical side, both atomic and nuclear. The extraction of the weak meson–nucleon couplings requires a good understanding of the atomic wave functions for the calculation of the matrix element and subtraction of additional radiative corrections as well as the nuclear structure to model the meson exchange inside the nucleus [125, 126].

5.3. Other optical atomic PNC proposals

Sanguinetti *et al* recently analysed in [147] a new proposal for PNC measurements with Fr. They suggest choosing a geometry where the laser beam exciting the transition is collinear to a slow, cold atomic beam, either extracted from a trap or prepared by Zeeman slower. This way the interaction time with the excitation laser is lengthened.

The observable that they propose is new in the atomic PNC experimental field. They suggest creating a spin polarization P_e of the atomic beam at the output of the trap in a direction perpendicular to its velocity. Then, an observable physical quantity is a contribution to the absorption rate involving this spin polarization. It results from an interference between the parity-violating electric dipole amplitude E_1^{PV} and the Stark amplitude induced by a transverse electric field. The manifestation of atomic PNC would rely on the presence in the absorption rate of the pseudoscalar quantity $(\mathbf{E} \times \xi \hat{\mathbf{k}}) \cdot \mathbf{P}_e$, where $\xi \hat{\mathbf{k}}$ represents the angular momentum of the light beam which excites the transition and \mathbf{E} is the applied static electric field. It has the advantage of appearing in the total population of the excited state. It can be detected by monitoring the total intensity of the fluorescence light emitted during the two-step de-excitation process. No polarization analysis or even light filtering (except for stray light) is necessary in principle. The PNC signal is odd under the separate reversals of the electric field, the spin polarization and the helicity of the photons which excite the transition.

The signal to noise ratios that they obtain are very promising and point to statistical precisions of 10^{-3} achievable with a beam of Fr of the order of one million atoms per second.

6. Perspectives and conclusions

This review shows the status of the work on francium and the understanding of its atomic structure. The experimental progress with francium has generated new ways to produce it, trap it and probe it. The agreement between experiment and theory in the lifetimes of different excited states is better than 1% and shows the quality and reliability of current day atomic structure calculations. This level of precision is comparable to other alkali species. The same theoretical methods used on other elements provide a cross check for the reliability of the calculations. This is a vital step in PNC studies where a theoretical calculation is required to extract the constants of the weak interaction from the measurement in caesium.

Francium has the potential of contributing to our understanding of the weak interaction directly. The size of the weak effects in francium are more than ten times larger than in caesium. In addition, the choice of different isotopes to work with opens new possibilities. Comparing the weak effects for different numbers of neutrons in the nucleus could provide a separation between weak interactions with protons or with neutrons. The study of the spin dependent part of the weak interaction through the anapole moment could provide access to weak processes among nucleons. The nucleons are strongly correlated at the low energies of atomic physics experiments and provide complementary information to that obtained at high energies.

Acknowledgments

This work has been supported by the United States National Science Foundation. EG acknowledges support from CONACYT.

Appendix. Tables of Fr parameters

The following tables summarize the parameters presented in this review and may become useful in future experiments with francium.

Table 5. ^{210}Fr trapping parameters.

Trapping energy ($7P_{3/2}$)	$13\,923.381 \pm 0.003 \text{ cm}^{-1}$
Repumping energy ($7P_{1/2}$)	$12\,238.425 \pm 0.003 \text{ cm}^{-1}$
I	6
$7S_{1/2}$ hyperfine splitting [39]	$46\,768.2 \pm 2.6 \text{ MHz}$
$A(7S_{1/2})$ [39]	$7195.1 \pm 0.4 \text{ MHz}$
$A(7P_{3/2})$ [148]	$78.0 \pm 0.2 \text{ MHz}$
$B(7P_{3/2})$ [148]	$51 \pm 0.4 \text{ MHz}$
$A(7P_{1/2})$ [28]	$946.3 \pm 0.2 \text{ MHz}$
Linewidth $7P_{3/2}$ $\Gamma/2\pi$	7.57 MHz
Linewidth $7P_{1/2}$ $\Gamma/2\pi$	5.40 MHz
Doppler temperature limit ($7P_{3/2}$)	$T_D = 182 \mu\text{K}$
Doppler velocity ($7P_{3/2}$)	$v_D = 8.4 \text{ cm s}^{-1}$
Recoil temperature limit ($7P_{3/2}$)	$T_r = 176 \text{ nK}$
Recoil velocity ($7P_{3/2}$)	$v_r = 2.6 \text{ mm s}^{-1}$
$I_{\text{sat}}(7P_{3/2})$ (two-level atom)	2.7 mW cm^{-2}
Radioactive half-life	3.2 min
Emitted alpha energy	6.54 MeV

Table 6. Measured lifetimes of electronic levels in Fr.

Level	τ (ns)
$7P_{1/2}$ [31]	29.45 ± 0.11
$7P_{3/2}$ [31]	21.02 ± 0.11
$7D_{3/2}$ [32]	73.6 ± 0.3
$7D_{5/2}$ [32]	67.7 ± 2.9
$8S_{1/2}$ [34]	53.30 ± 0.44
$8P_{1/2}$ [95]	149.3 ± 3.5
$8P_{3/2}$ [95]	83.5 ± 1.5
$9S_{1/2}$ [95]	107.53 ± 0.90

Table 7. The measured energy levels of Fr. Energies are given in (cm^{-1}) and relative to the ground state. The numbers are for low lying states of three different isotopes 210, 212 and 221.

Isotope level	Energy (cm^{-1})		
	^{210}Fr	^{212}Fr	^{221}Fr
$7S_{1/2}$	0	0	0
$7P_{1/2}$ [35, 149]		$12\,237.409 \pm 0.002$	$12\,236.6579 \pm 0.017$
$7P_{3/2}$ [35, 149]		$13\,923.998 \pm 0.002$	$13\,923.2041 \pm 0.017$
$8S_{1/2}$ [27]	$19\,732.523 \pm 0.004$		
$8P_{1/2}$ [150]		$23\,112.960 \pm 0.005$	
$8P_{3/2}$ [150]		$23\,658.306 \pm 0.004$	
$7D_{3/2}$ [29]	$24\,244.831 \pm 0.003$		
$7D_{5/2}$ [29]	$24\,333.298 \pm 0.003$		
$9S_{1/2}$ [26]	$25\,671.021 \pm 0.006$		
$8D_{3/2}$ [38]		$27\,600.657 \pm 0.007$	
$8D_{5/2}$ [38]		$27\,645.373 \pm 0.007$	
$10S_{1/2}$ [38]		$28\,310.617 \pm 0.006$	
$9D_{3/2}$ [38]		$29\,316.497 \pm 0.007$	
$9D_{5/2}$ [38]		$29\,341.817 \pm 0.007$	

Table 7. (Continued.)

Isotope level	Energy (cm ⁻¹)		
	²¹⁰ Fr	²¹² Fr	²²¹ Fr
11S _{1/2} [38]		29 718.909 ± 0.006	
10DS _{3/2} [38]		30 309.962 ± 0.006	
10DS _{5/2} [38]		30 325.605 ± 0.006	
12S _{1/2} [38]		30 559.504 ± 0.006	
11D _{3/2} [38]		30 936.325 ± 0.006	
11D _{5/2} [38]		30 946.643 ± 0.006	
13S _{1/2} [38]		31 101.539 ± 0.006	
12D _{3/2} [38]		31 356.506 ± 0.006	
12D _{5/2} [38]		31 363.655 ± 0.006	
14S _{1/2} [38]		31 471.465 ± 0.006	
13D _{3/2} [38]		31 652.000 ± 0.006	
13D _{5/2} [38]		31 657.155 ± 0.006	

Table 8. Measured energy levels of ²¹²Fr in high excited states. Energies are given in cm⁻¹ and relative to the ground state.

Level	Energy (cm ⁻¹)
15S _{1/2} [38]	31 735.182 ± 0.006
14D _{3/2} [38]	31 867.682 ± 0.006
14D _{5/2} [38]	31 871.514 ± 0.006
16S _{1/2} [38]	31 929.789 ± 0.006
15D _{3/2} [38]	32 029.909 ± 0.006
15D _{5/2} [38]	32 032.821 ± 0.006
17S _{1/2} [38]	32 077.492 ± 0.006
16D _{3/2} [38]	32 154.979 ± 0.006
16D _{5/2} [38]	32 157.274 ± 0.006
18S _{1/2} [38]	32 192.251 ± 0.006
17D _{3/2} [38]	32 253.449 ± 0.006
17D _{5/2} [38]	32 255.275 ± 0.006
19S _{1/2} [38]	32 283.180 ± 0.006
18D _{3/2} [38]	32 332.354 ± 0.006
18D _{5/2} [38]	32 333.827 ± 0.006
20S _{1/2} [38]	32 356.444 ± 0.006
19D _{3/2} [38]	32 396.552 ± 0.006
19D _{5/2} [38]	32 397.761 ± 0.006
21S _{1/2} [38]	32 416.340 ± 0.006
20D _{3/2} [38]	32 449.483 ± 0.006
20D _{5/2} [38]	32 450.488 ± 0.006
22S _{1/2} [38]	32 465.937 ± 0.006
Ionization limit [38]	32 848.872 ± 0.009

References

- [1] Metcalf H J and van der Straten P 1999 *Laser Cooling and Trapping* (New York: Springer)
- [2] Sprouse G D and Orozco L A 1997 *Ann. Rev. Nucl. Part. Sci.* **47** 429
- [3] Scielzo N D, Freedman S J, Fujikawa B K and Vetter P A 2004 *Phys. Rev. Lett.* **93** 102501

- [4] Gorelov A *et al* 2005 *Phys. Rev. Lett.* **94** 142501
- [5] Crane S G, Brice S J, Goldschmidt A, Guckert R, Hime A, Kitten J J and Vieira D J and Zhao X 2001 *Phys. Rev. Lett.* **86** 2967
- [6] Sapirstein J 1998 *Rev. Mod. Phys.* **70** 55
- [7] Ginges J S M and Flambaum V V 2004 *Phys. Rep.* **397** 63
- [8] Bouchiat M A and Bouchiat C 1997 *Rep. Prog. Phys.* **60** 1351
- [9] Bouchiat M A and Bouchiat C 1974 *J. Phys. (Paris)* **35** 899
- [10] Wood C S, Bennett S C, Cho D, Masterson B P, Roberts J L, Tanner C E and Wieman C E 1997 *Science* **275** 1759
- [11] Vetter P A, Meekhof D M, Majumder P K, Lamoreaux S K and Fortson E N 1995 *Phys. Rev. Lett.* **74** 2658
- [12] Budker D 1998 *Physics Beyond the Standard Model* (Singapore: World Scientific)
- [13] Macpherson M J D, Zetie K P, Warrington R B, Stacey D N and Hoare J P *Phys. Rev. Lett.* **67** 2784
- [14] DeMille D 1995 *Phys. Rev. Lett.* **74** 4165
- [15] Fortson N 1990 *Phys. Rev. Lett.* **765** 2857
- [16] Pollock J, Fortson E N and Wilets L 1992 *Phys. Rev. C* **46** 2587
- [17] Blundell S A, Johnson W R and Sapirstein J 1991 *Phys. Rev. A* **43** 3407
- [18] Dzuba V A, Flambaum V V and Sushkov O P 1989 *Phys. Lett. A* **141** 147
- [19] Langacker P (ed) 1995 *Precision Tests of the Standard Electroweak Model* (Singapore: World Scientific)
- [20] Peskin M E 1998 *Science* **281** 1153
- [21] Erler J and Langacker P 2000 *Phys. Rev. Lett.* **84** 212
- [22] Rosner J L 2002 *Phys. Rev. D* **65** 0073026
- [23] Derevianko A 2000 *Phys. Rev. Lett.* **85** 1618
- [24] Liberman S *et al* (ISOLDE Collaboration) 1978 *C R Acad. Sci. B* **286** 253
- [25] Simsarian J E, Ghosh A, Gwinner G, Orozco L A, Sprouse G D and Voytas P A 1996 *Phys. Rev. Lett.* **76** 3522
- [26] Simsarian J E, Shi W, Orozco L A, Sprouse G D and Zhao W Z 1996 *Opt. Lett.* **21** 1939
- [27] Simsarian J E, Zhao W Z, Orozco L A and Sprouse G D 1999 *Phys. Rev. A* **59** 195
- [28] Grossman J S, Orozco L A, Pearson M R, Simsarian J E, Sprouse G D and Zhao W Z 1999 *Phys. Rev. Lett.* **83** 935
- [29] Grossman J M, Fliller III R P, Mehlstäubler T E, Orozco L A, Pearson M R, Sprouse G D and Zhao W Z 2000 *Phys. Rev. A* **62** 052507
- [30] Zhao W Z, Simsarian J E, Orozco L A, Shi W and Sprouse G D 1997 *Phys. Rev. Lett.* **78** 4169
- [31] Simsarian J E, Orozco L A, Sprouse G D and Zhao W Z 1998 *Phys. Rev. A* **57** 2448
- [32] Grossman J M, Fliller III R P, Orozco L A, Pearson M R and Sprouse G D 2000 *Phys. Rev. A* **62** 062502
- [33] Aubin S, Gomez E, Orozco L A and Sprouse G D 2004 *Phys. Rev. A* **70** 042504
- [34] Gomez E, Orozco L A, Galvan A P and Sprouse G D 2005 *Phys. Rev. A* **71** 062504
- [35] Lu Z T, Corwin K L, Vogel K R, Wieman C E, Dinneen T P, Maddi J and Gould H 1997 *Phys. Rev. Lett.* **79** 994
- [36] Atutov S N *et al* 2004 *Nucl. Phys. A* **746** 421c
- [37] Perey M 1939 *C. R. Acad. Sci.* **208** 97
- [38] Arnold E *et al* (ISOLDE Collaboration) 1990 *J. Phys. B* **23** 3511
- [39] Coc A *et al* (ISOLDE Collaboration) 1985 *Phys. Lett. B* **163** 66
- [40] Andreev S V, Mishin V I and Letokhov V S 1988 *J. Opt. Soc. Am. B* **5** 2190
- [41] Dinneen T, Ghiorso A and Gould H 1996 *Rev. Sci. Instrum.* **67** 752
- [42] Lettry J *et al* 1997 *Nucl. Instrum. Methods B* **326** 170
- [43] Gwinner G, Behr J A, Cahn S B, Ghosh A, Orozco L A, Sprouse G D and Xu F 1994 *Phys. Rev. Lett.* **72** 3795
- [44] Lipski A R, Orozco L A, Pearson M R, Simsarian J E, Sprouse G D and Zhao W Z 1999 *Nucl. Instrum. Methods A* **438** 217
- [45] Behr J A, Cahn S B, Dutta S B, Ghosh A, Gwinner G, Holbrow C H, Orozco L A, Sprouse G D, Urayama J and Xu F 1994 *Nucl. Instrum. Methods A* **351** 256
- [46] Melconian D *et al* 2005 *Nucl. Instrum. Methods A* **538** 93
- [47] Monroe C, Swann W, Robinson H and Wieman C 1990 *Phys. Rev. Lett.* **65** 1571
- [48] Lu Z T, Bowers C T, Freedman S J, Fujikawa B K, Mortara J L, Shang S Q, Coulter K P and Young L 1994 *Phys. Rev. Lett.* **72** 3791
- [49] Goldenberg H M, Kleppner D and Ramsey N F 1961 *Phys. Rev.* **123** 530
- [50] Vanier J, Simard J F and Boulanger J S 1974 *Phys. Rev. A* **9** 1031
- [51] Swenson D R and Anderson L W 1988 *Nucl. Instrum. Methods B* **29** 627
- [52] Stephens M, Rhodes R and Wieman C 1994 *J. Appl. Phys.* **76** 3479
- [53] Atutov S N *et al* 2003 *J. Opt. Soc. Am. B* **20** 953

- [108] Barkov L M and Zolotarev M S 1979 *Phys. Lett. B* **85** 308
- [109] Bucksbaum P H, Commins E D and Hunter L R 1981 *Phys. Rev. D* **24** 1134
- [110] Prescott C Y *et al* 1978 *Phys. Lett. B* **77** 347
- [111] Arnison G *et al* (UA1 Collaboration) 1983 *Phys. Lett. B* **122** 103
- [112] Arnison G *et al* (UA1 Collaboration) 1983 *Phys. Lett. B* **126** 398
- [113] Wood C S, Bennett S C, Roberts J L, Cho D and Wieman C E 1999 *Can. J. Phys.* **77** 7
- [114] Milstein A I and Sushkov O P 2002 *Phys. Rev. A* **66** 022108
- [115] Johnson W R, Bednyakov I and Soff G 2001 *Phys. Rev. Lett.* **87** 233001
- [116] Kuchiev M Y and Flambaum V V 2002 *Phys. Rev. Lett.* **89** 283002
- [117] Milstein A I, Sushkov O P and Terekhov I S 2002 *Phys. Rev. Lett.* **89** 283003
- [118] Harber D M, Lewandowski H J, McGuirk J M and Cornell E A 2002 *Phys. Rev. A* **66** 053616
- [119] Langacker P, Luo M and Mann A K 1992 *Rev. Mod. Phys.* **64** 87
- [120] Peskin M E and Takeuchi T 1990 *Phys. Rev. Lett.* **65** 964
- [121] Peskin M E and Takeuchi T 1992 *Phys. Rev. D* **46** 381
- [122] Abe F *et al* (CDF Collaboration) 1997 *Phys. Rev. Lett.* **79** 2192
- [123] Cheung K 2001 *Phys. Lett. B* **517** 167
- [124] Khriplovich I B 1991 *Parity Nonconservation in Atomic Phenomena* (New York: Gordon and Breach)
- [125] Flambaum V V and Murray D W 1997 *Phys. Rev. C* **56** 1641
- [126] Haxton W C and Wieman C E 2001 *Annu. Rev. Nucl. Part. Sci.* **51** 261
- [127] Fortson N 1993 *Phys. Rev. Lett.* **70** 2383
- [128] Zel'dovich Y B 1958 *Sov. Phys.—JETP* **6** 1184
- [129] Flambaum V V, Khriplovich I B and Sushkov O P 1984 *Phys. Lett. B* **146** 367
- [130] Bouchiat M A and Bouchiat C C 1974 *Phys. Lett. B* **48** 111
- [131] Bouchiat M A and Bouchiat C 1975 *J. Phys. (Paris)* **36** 493
- [132] Bouchiat M A and Bouchiat C 2001 *Eur. Phys. J. D* **15** 5
- [133] Meekhof D M, Vetter P, Majumder P K, Lamoreaux S K and Fortson E N 1993 *Phys. Rev. Lett.* **71** 3442
- [134] Meekhof D M, Vetter P, Majumder P K, Lamoreaux S K and Fortson E N 1995 *Phys. Rev. A* **52** 1895
- [135] Guéna J, Chauvat D, Jacquier P, Jahier E, Lintz M, Sanguinetti S, Wasan A, Bouchiat M A, Papoyan A V and Sarkisyan D 2003 *Phys. Rev. Lett.* **90** 143001
- [136] Stalnaker J E, Budker D, DeMille D P, Freedman S J and Yashchuk V V 2002 *Phys. Rev. A* **66** 031403
- [137] Koerber T W, Schacht M, Nagourney W and Fortson E N 2003 *J. Phys. B* **36** 637
- [138] DeMille D P 2005 <http://pantheon.yale.edu/~7Edpd5/demille.research.htm>
- [139] Ezhov V F *et al* <http://www.qchem.pnpi.spb.ru/publication/Report01/rep.html>
- [140] Orozco L A 2002 *Trapped Particles and Fundamental Physics, Les Houches* ed S N Atutov *et al* (Amsterdam: Kluwer)
- [141] Gomez E, Aubin S, Orozco L A, Sprouse G D and DeMille D 2004 *Preprint physics/0412124*
- [142] Loving C E and Sandars P G H 1977 *J. Phys. B* **10** 2755
- [143] Gorshkov V G, Ezhov V F, Kozlov M G and Mikhailov A I 1988 *Sov. J. Nucl. Phys.* **48** 867
- [144] Hinds E A and Hughes V W 1977 *Phys. Lett. B* **67** 487
- [145] Adelberger E G, Traino T A, Fortson E N, Chupp T E, Holmgren D, Iqbal M Z and Swanson H E 1981 *Nucl. Instrum. Methods* **179** 181
- [146] Itano W M, Begquist J C, Bollinger J J, Gilligan J M, Heinzen D J, Moore F L, Raizen M G and Wineland D J 1993 *Phys. Rev. A* **47** 3554
- [147] Sanguinetti S, Guéna J, Lintz M, Jacquier P, Wasan A and Bouchiat M A 2003 *Eur. Phys. J. D* **25** 3
- [148] Liberman S *et al* 1980 *Phys. Rev. A* **22** 2732
- [149] Bauche J *et al* (ISOLDE collaboration) 1986 *J. Phys. B* **19** 593
- [150] Duong H T *et al* (ISOLDE Collaboration) 1987 *Europhys. Lett.* **3** 175